**Republic of Iraq**

**Ministry of Higher Education**

**And Scientific Research**

**University Of Misan**

**College of Science**

# Preparation of Injectable Calcium Phosphate Bone Cement Extracted from Marine Fishes and Bovine Bone for Potential Orthopedic Applications

A Thesis Submitted to

the College of Science / University of Misan as Partial Fulfillment

of the Requirements for the Master Degree of Science in Chemistry

By

**Kholoud Jabar Wali**

B.Sc. Chemistry / Basrah University (2002)

Supervisor

***Asst. Prof. Dr*. Ali Taha Saleh**

2024

بِسْمِ اللهِ اَلَّرَحْمنِ اَلَّرَحْيم

« يَرْفَعُ اللهُ الَّذِينَ آمَنُوا مِنْكُمُ والَّذِينَ أُوْتُوا الّعِلْمَ دَرَجّاتٍ وَاللهُ بِمْآ تَعّلَمُونَ خَبِيرِ »

صَدَقَ اللهُ الّعَلِيُ الّعَظْيِم

" سورةالمجادلة .... الآية (11) "

# Dedication

To Whom I can never forget, the one who's passing away made me sad, and my constant grief ….

***My father*** "my God have mercy on him"

To The source of tenderness in my life, who illuminates the shadows of difficulties with her prayers ….

***My mother***

To The Happiness Buds, The Hope of my life M. Baqer, and Rawan ….

***My husband and Childrens***

To Those how have supported me and waiting for my Success ….

***My Brothers & My close Friends***

To The one who has given me his knowledge ….

***My superviso***

# *Acknowledgements*

Praise be God And thanks be to Him as it should be for the majesty of His countenance, the greatness of His authority, the number of His creation, the contentment of Himself, the weight of His Throne, and the supply of His words, who gave me health, strength, and facilitated the ways for me to accomplish this work, and the prayer and peace of Allah be upon our Master and prophet Muhammad and his divine good family.

I would like to express my sincere gratitude to my supervisors, **Asst. Prof. Dr. Ali Taha Saleh** for highly inspiring guidance, patience, motivation, enthusiasm and immense knowledge, continuous support for completing this thesis.

Also, I express my sincere thanks and gratitude to my family for their help mein providing the appropriate ambiences for study.

Finally, I'd like to thank my post graduate classmates, best friends, another family for supported me and stand with me, apology to all whom I have not mentioned with my respect. thanks for all.

*Researcher*

# Contents

# Contents

# Contents

# Contents

# List of Figures

# List of Figures

# List of Tables

# List of Tables

# List of Abbreviations

| Abbreviations | Key |
|---|---|
| HA | Hydroxyapatite |
| TCP | Tricalcium Phosphate |
| CaP | Calcium Phosphate cement |
| CPC | Calcium Phosphate |
| CDHA | Calcium-deficient |
| CS | Compression Strength |
| βTCP | β- Tricalcium Phosphate |
| SBF | Simulated body fluid |
| BG | Bioactive Glasses |
| BCP | Biphasic Calcium Phosphate |
| MW | Microwave |
| MCPM | Monocalcium phosphate monohydrate |
| MCPA | Monocalcium phosphate anhydrous |
| MCP | Monocalcium phosphate anhydrous |
| DCPD | Dicalcium phosphate dihydrate (Brushite) |
| DCPA | Dicalcium phosphate anhydrous (Monetite) |
| OCP | Octacalcium Phosphate |
| αTCP | α-Tricalcium Phosphate |

# List of Abbreviations

| Abbreviations | Key |
|---|---|
| TTCP | Tetracalcium Phosphate |
| ACP | Amorphous calcium phosphate |
| FWHM | Full width at half maximum |
| DDW | Doubled distilled water |
| FTIR | Fourier Transform Infrared Spectroscopy |
| XRD | X-Ray diffraction |
| EDX | Energy-dispersive X-ray spectroscopy |
| FESEM | Field Emission Scanning Electron Microscope |
| TEM | Transmission electron microscopy |
| UV | Ultraviolet Light |
| ICP-MS | Inductively coupled plasma mass spectrometry |
| LB | Luria-Bertani |
| SD | Standard deviation |

# List of Symbols

| Symbols | Key |
|---|---|
| e.g | For Example, |
| etc | Et Cetera |
| 3D | Three-Dimensional |
| mol% | Percentage of Number of Moles |
| Ca/P | Calcium to Phosphate Ratio |
| wt% | Weight-Weight Percentage |
| ppm | Part Per million |
| µm | Micrometer |
| i.e. | In other words, |
| Å | Angstrom |
| °C | Temperature |
| Nm | Nanometers |
| 2θ | 2 Theta |
| mM | Millimole |
| M | Molarity |
| min | Minutes |
| H | Hours |
| eV | Electron Volt |
| mg/L | Milligram Per Liter |
| Xc | Degree of Crystallinity |
| m2/g | Square Meter per Gram |
| P/L | Powedr / liquid |

**Abstract**

The project is divided into three chapters. The first provides a broad overview of biological hydroxyapatite extraction from natural sources for use in biomedical applications. The experimental procedure, including sample preparation, hydroxyapatite extraction, and calcium phosphate cement preparation, is covered in the second chapter. The findings and commentary are covered in the final chapter. This research used a variety of newly extracted hydroxyapatite (HA) from fish bones in the Arabian Gulf of Basrah, Iraq, and bovine bone from Misan City, Iraq, as natural sources of bones. by using the process of calcination at various temperatures. Because of its capacity to be reabsorbed under physiological settings, calcium phosphate cements (CPC) are often chosen over alternative calcium phosphate-based biomaterials in orthopedic procedures. The emphasis of current cement development techniques for calcium phosphate is on in-situ setting of the cements under physiological settings with suitable mechanical characteristics. The phase composition, surface morphology, and chemical composition of hydroxyapatite (HA) calcium phosphate cement were assessed by means of X-ray diffraction (XRD), field emission scanning electron microscopy (FESEM) coupled with energy dispersive X-ray analysis (EDX), X-ray, and Fourier transform infrared spectroscopy (FTIR) techniques. We assessed the cement's in vitro dissolving behavior by submerging the samples in simulated bodily fluid (SBF) for seven days at 37 °C.

# CHAPTER ONE

# INTRODUCTION

## 1.1 Overview

Waste products derived from natural resources are valuable chemicals recovered. It takes certain methods and approaches to turn such waste products into valuable resources. One biomaterial that may be obtained from herbal wastes is hydroxyapatite $Ca_{10}(PO_4)_6(OH)_2$(HA). Due to its excellent osteoconduction trends, high biocompatibility, and outstanding bioactivity, HA has found extensive utility in biomedical applications , because of this, HA is becoming more and more popular in produced dental materials and orthopedic implants. The methods now used to extract HA from herbal resources include minerals, shells, aquatic or marine resources, mammals, plants, and algae. Additionally, the methods for extracting hydroxyapatite are explained. This document cites the device and herbal waste source on the key HA houses.

## 1.2 Human Bone

Nonstoichiometric calcium phosphates (CaP) together with trace amounts of other ions make up the unique composition of bone [1] . Bone is a somewhat ordered polymer/ceramic nanocomposite that provides shape to the frame's skeleton [1]. It serves as a great reservoir for various minerals including calcium and phosphate in addition to its structural support of the body [2]. Bone is a dynamic material with the unusual capacity to self-organize or regenerate to a positive volume till the end. There are two kinds of bones: one is the cortical bone, also known as the compact bone, and the other is the trabecular bone, also known as the cancellous or spongy bone. These types are divided into groups according to their unit microstructure and porosity [3]. Long bones often include cortical bone

in their shafts. With five to ten percent porosity, it's a very thick form. It is seen at the end of joints as the outer shell around the cancellous bone [4]. Based on their microstructure, certain types of cortical bones may be distinguished from one another. Compared to trabecular bone, cancellous bone is more porous, ranging from 50% to 90%. It may be found within vertebrae, at the end of long bones, and on flat bones [5].

## 1.3 Main inorganic components of bones.

Various types of HA with different properties, that can be used for specific applications, may be synthesized from numerous sources. Depending on the crystal phase, e.g., CaP ceramics can be classified as hydroxyapatite HA [($Ca_{10}(PO_4)_6(OH_2)$), Ca/P=1.67];precipitated hydroxyapatite pHA [$Ca_{10-x}(HPO_4)_x(PO_4)_{6-x}(OH)_{2-x}$,x=1.50–1.67] calciumdeficient hydroxyapatite CDHA [$Ca_{10-x}(HPO_4)_x(PO_4)_{6-x}(OH)_{2-x}$, x=1.50–1.67] Due to its near chemical and crystallographic structural resemblance to the inorganic components of teeth and bones. HA and its combination with TCP are commonly employed as bone substitution materials and coatings on dental implants. [7–12] Moreover, CaP ceramics' exceptional bioactivity, biocompatibility, non-toxicity, non-immunogenicity, and non-inflammatory behavior make them essential materials for hard tissue restoration [1, 2].

## 1.4 Biomaterials

Because of the growing ageing population and the treatment of illnesses, biomaterials have been gaining importance. Research on the creation of novel materials or the configuration and shaping of biomaterials has been heavily focused on home décor [13]. As implants, napkins, and member engross and distribution structures, the user is usually favored [6]. One effective method of extending life expectancy is by biological restoration, repair, or updating of the damaged tissue through integration with the intricate structure [14]. Depending on their biocompatibility and other characteristics, biomaterials may be used in a variety of packages due to their diverse mechanistic, physiological, alchemical, and constitutional homes. One class of materials found in biomedical devices are ceramics [15]. Because ceramics may mimic a diffusion process with high compressive strength, they are often employed as implant materials because they are physiologically hospitable and changeable [16]. The increasing similarity between the chemical composition of calcium phosphate and some ceramics [17]. These materials exhibit exceptional bioactivity, high levels of biocompatibility, and amazing [18]. Even yet, treating bone disorders resulting from long-term illness or trauma remains a challenge for medical professionals. In addition to the necessary duration, the treatment of skeletal illnesses often necessitates the use of synthetic biological materials [19]. due to the limited supply of (tissues or cells) taken from the same person. The use of artificial biomaterials, tissue grafts, organ transplants from donors of a different species than the recipient, and bone sections from certain types of brutes are crucial because to the risk of viable contamination from the use of allographt [18, 20 The closely resembles the form and structure of the human skeleton. Bones from cattle, sheep, pigs, or fish are used to create

xenografts, which contain a large number of valuable ions that can easily be obtained in bulk deliveries and need inexpensive transference [21]. Xenogenous materials may withstand a removal process that involves heating them to higher temperatures.

## 1.5 Calcium Phosphates $Ca_3(PO_4)_2$

Like metals determined at loftiness, calcium phosphates are crystal ceramics with an alchemical texture and structure. One often used model of calcium phosphate is called Hap, which is based on the chemical formulation and has a structure similar to the main metals found in bone, apatite [22].

Because of its real biocompatibility, bioactivity, high osteoconductive and/or osteoinductive ability, nontoxicity, and residences, HA is suited for employment as a loftiness filler and as a covering on prostheses [23]. It seems that floor price scaffolding is connected to the promotion of osteogenesis and osteointegration that calcium phosphate scaffolds are said to foster [24]. Nevertheless, the resorption price of this ceramic is modest. Consequently, other calcium phosphates were developed, including β-tricalcium phosphate, which has a quick resorption rate. As a backup, current calcium phosphate sources have been investigated (Fig. 1.1). Seashells, algae, corals, fish bones, and other unique marine sources may all be used to extract calcium phosphates. Because the skeleton of sponges belonging to the phylum Porifera is made of bioceramics, which is comparable to bone in terms of its mechanical, osteoconductive, and resorbable qualities, new techniques have been developed in order to study them [25]. You can get this lovely cloth in stores [26].

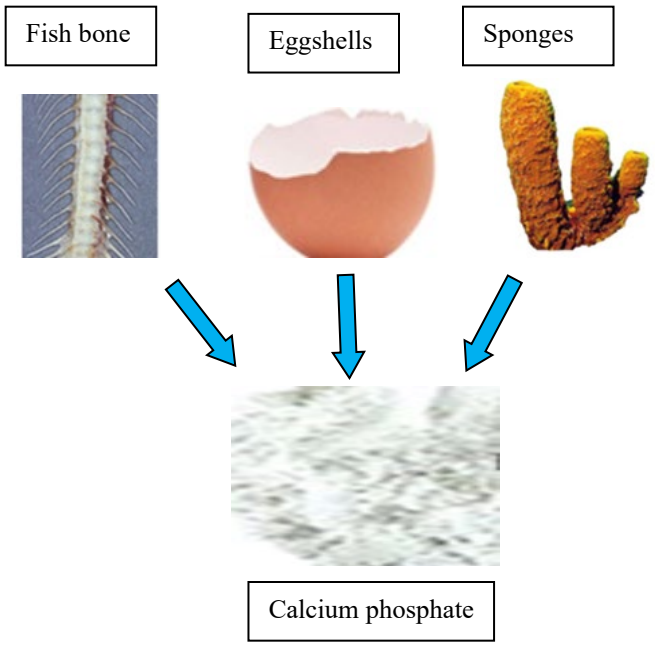


**Figure 1.1**: Some sources of calcium phosphate

## 1.6 Hydroxyapatite (HA)

HA molecular structure: $Ca_{10}(PO_4)_6(OH)_2$. Those bioceramics may be intentionally synthesized using special techniques, such as precipitation, hydrothermal, multiple emulsion, biomimetic deposition, and electrodeposition techniques [28]. They crystallize into the hexagonal device (figure 1.2) [27]. Moreover, appropriately produced using the sol gel method, which combines certain precursors of phosphorus and calcium to produce an excessively pure HA at the molecular level [28, 29]. Given the possibility for synthetic manufacture to be improved, HA may also be removed from the skeleton template, wherever it is naturally established in large quantities. Undoubtedly, the mineral additives that make approximately 70–80% of the noncellular skeletal template provide a tremendous amount of mechanical electricity [30]. A Ca/P ratio of less than 1.67 is opposed by normal HA, and its uneven nanostructured crystal contains

carbonate companies and strains of several ions, such as $HPO^{2}_{4}$, $Na^{+}$, $Mg^{2+,}$ $Sr^{2+}$, $k^{+}$, $Cl^{-}$, and $F^{-}$, inside of it [31].

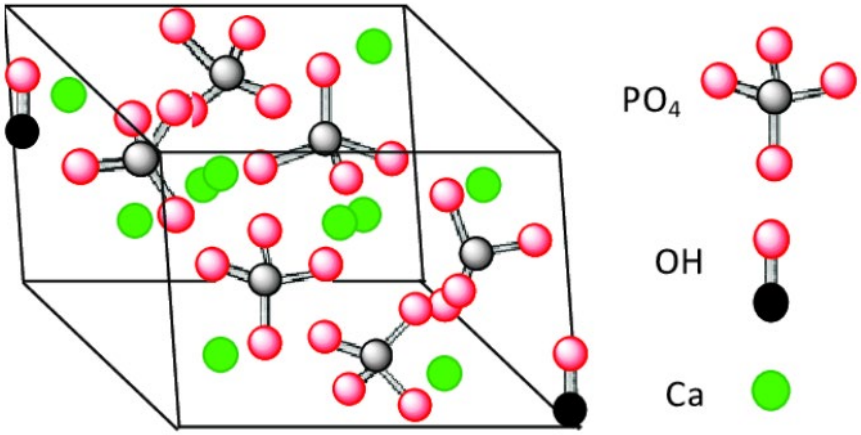


**Figure 1.2:** Crystal structure of hydroxyapatite

## 1.7 Compounds related to Hydroxyapatite

Compounded mostly of calcium phosphate (CP), these compounds have a Ca/P molar proportion within the range 0.5–2 [32] and are the extreme in demand biomaterials for the rebuilding of many skeletal issues, particularly inside the scope of dentistry, orthopedic and shock surgical treatment [33, 34]. A short list of crucial CP-based totally ceramic materials in conjunction with their formulas and packages is offered in table 1. Owing to their exceptional biocompatibility [35, 36], osteoconductivity [37], and osteointegration [38], compounds principally derived from CP have been the subject of much investigation over the last fifty years. Biomaterials that are largely CP-established are appropriately used to replace and strengthen the strong tissues of the epidermis frame that are damaged or deteriorating.

The term "apatite" is often used to describe CPs' magnificent reign trendy

technique, in which A and B are regarded as calcium in many distinct residences that are special to phosphate institutions, and X denotes the subsistence of OH-organization within form [40]. HA is an important CP-primarily initiated chemical that resembles a metal element found in enamel and herbs [41]. HA with bioactivity [43] and a Ca/P ratio of [42]. It has been used for more than 50 years as a dental grow and as a bone exchange fabric [44]. Because of its osteoconductive immovables, HA can elevate fast bone renewal and immediate bonding with remade bone without the need of moderate conjunctive tissues. Its artificial shape primarily used to remodel strict environments, such as strict textile reconstruction [45]. due to HA's growing importance as a biomaterial, attempts are constantly made to make HA's organic homes more beautiful. In spite of the fact that HA extensively in the area of orthopedics, their rating of deterioration in the physiological environment restricts their use in clinical settings. [46] Research has shown that adding biocompatible ions to HA ion-pleasant crystal structure may modify the degradation average of the compound [47].

**Table 1**: Ca/P ratio of biomaterials

| No. | Compounds | Formula | Ellipsis | Ca/p |
|---|---|---|---|---|
| 1 | Monocalcium phosphate monohydrate | $Ca(H_2PO_4)_2.H_2O$ | MCPM | 0.5 |
| 2 | Monocalcium phosphate (anhydrous) | $Ca(H_2PO_4)_2$ | MCPA | 0.5 |
| 3 | calcium phosphate (anhydrous) | $CaHPO_4$ | DCPA | 1 |
| 4 | Monocalcium phosphate dehydrate | $CaHPO_4.2H_2O$ | DCPD | 1 |
| 5 | β-Tricalcium phosphate | $Ca_3(PO_4)_2$ | TCP | 1.5 |
| 5 | Hydroxyapatite | $Ca_{10}(PO_4)_6(OH)_2$ | HA | 1.67 |
| 6 | Tetracalcium phosphate | $Ca_4(PO_4)_{2O}$ | TTCP | 2 |

In its crystalline state, hydroxyapatite exhibits remarkable thermodynamic properties [48]. Without resulting in any localized or systemic toxicity, infection, or foreign frame response, HA may mix with bone [49]. These factors have led to the widespread use of HA in biomedical packaging, and orthopedics, [20, 50]. A great deal of research has been done on methods for creating HA that may be modified. Conventional chemical methods lack the necessary HA assembly signal of beneficial components such as silicon, barium, sodium, zinc, and fluorine ions, among others; the presence of those ions directly affects a number of biological processes connected to bone metabolism. The assembly description and use of ion-substituted HA were accurately depicted in recently published research publications [54]. Ions have the ability to interchange all of the OH- or $PO_4^{3-}$, The often point out to as A-type or B-type replacement, or they may replace the Ca ions within the crystalline structure. Less costly natural organic reservoirs, including as fish and mammal bones [55], corals, eggshells, seashells, and flora, have made it possible to create ready-made ion-doped HA in an appealing and effective way [56].

## 1.8 Natural hydroxyapatite

The majority of normal HA is prepared from several wastes concurrently with the skeleton of mammals (e.g., vaccine, garnish, and steed), the skeleton of fish and other aquatic animals (e.g., fish skeleton), the sources of cortex (e.g., crinkle, clam, and mother-of-pearl), the existence of seeds, moss, and metallic exchequer (e.g. limestone). The exchequer and some instances of the methods utilized to synthesize inbred HA are shown in Fig. 1.4 [57]. In essence, stoichiometric HA is contain of Ca and P, with a grinder ratio one to sixty-seven [58]. It has been shown that this ratio is unique for bone regeneration sales [53, 59]. Herbs are low in phosphorus and calcium. The most frequent empty spaces in HA are called calcium locations, and they contain cations [60] [37].

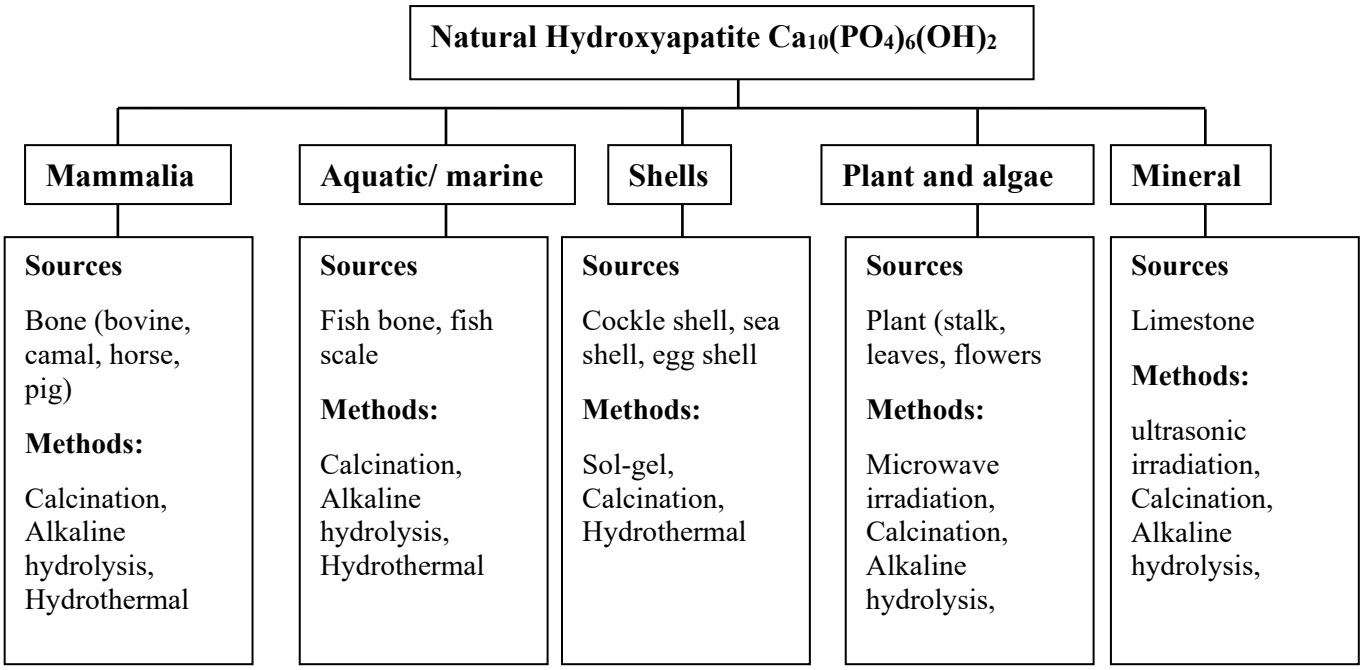


**Figure.1.3:** outline of methods for synthesizing natural HA

## 1.9 Organic assets for the preparing of hydroxyapatite

### 1.9.1 Preparing of hydroxyapatite from mammalian bones

When compared to other supplies such as garnish, steed, and swinish, the descent of hydroxyapatite for vaccine loftiness became often proposed in appropriateness among mammalian resources. To be morphologically and structurally similar to the epidermal skeleton, the cortical component of the femoral loftiness is often used [61], the Ca/P ratio, length, architectures, and Ca-P crystal levels. The homes differ based on the parent that was exercised and the extraction strategies that were used; hence, the data includes calcification heat and PH [58]. Maximum urbanity is often seen as having a significant impact on how loftiness is treated [41]. The information includes lotion while eliminating the dirt, fat, albuminoid, and other contaminants, such as loftiness squash and soft tissues. A few studies have discussed the use of an ebullience bath to eliminate natural components of the skeleton for up to eight hours [62]. A concoction of lotion and seethe combined with solvents, acetone, and chloroform celebrates loftiness [63]. The alternative pretreatment method, which has been widely used, involves irrigating the loftiness instead of the surfactant and using alkali to remove the smooth tissues while decellularizing it [43]. Bones also breaks into little parts before or after the necessary components are removed. Maximum plurality of urbanity suggested with an opinion that the bone was severed headfirst until minimal portions were removed before boiling or treated with a solvent to losing undesirable additives, like loftiness squash that was inside the skeleton [43, 64]. The majority of strategies used the calcification method, which is either the lone or a collection of calcifications at other strategies, until the ancestor of hydroxyapatite

for mammalian loftiness. The process of calcination involves heating the material to temperatures as high as 1400 C in an oven in order to completely destroy any potential germs while also eliminating any natural materials [65].

### 1.9.2. Hydroxyapatite from bovine bone

Hydroxyapatite taken away from vaccine cortical loftiness has been utilized to manufacture scaffolding. The aggregation of Hydroxyapatite crystals in the extracellular template of the vaccine skeleton has been the focus of several investigations into the origins of herbal HA [68]. It is affordable and hygienic to remove hydroxyapatite from a typical loftiness drome. Bone is unique mixed molding (weight nine percent), and natural themes include modest amounts of lipids, proteins, and carbohydrates. [69].

Using calcification vaccine femur, lamb femur loftiness, lamb crown marionette loftiness, and fowl femur bone between six hundred and one hundred $^{o}$C, thermally strong segment hydroxyapatite was produced [70]. The segment-natural crystalline HA with a crystallite size of about 133 nm was produced by the 800 C calcification process [57]. Growth during calcification fever to 1100 C extended the Hydroxyapatite's crystallinity; however, such rising calcification heat resulted in the formulation of TCP. The common crystallite length (fifty-eight. Four nm) was calculated using the Scherrer equation, and the XRD spectra calcification at summary heat was the reason given for the development of derivative stages like CaO and Ca $(OH)_2$ [59].

To extract HA from mammalian bone, further methods have been used in conjunction with an alkaline warming treatment. In this method, the organic count

is eliminated by using the alkaline solution NaOH. The natural problem in the bone is hydrolyzed by the NaOH solution, and the remaining calcium phosphate is washed and removed by filtering. But alkaline heat treatment is more effective than calcination [71]. readily apparent for calcined HA [74].

### 1.9.3 Hydroxyapatite HA from fish bone

HA has been attributed to fish, which is subsequently utilized as a basic material in the HA extraction process, according to a number of published accounts. Mustafa et al. isolated a purified phase of HA from tilapia (Oreochromis niloticus) fish bones subjected to 900 °C. Biphasic calcium phosphate was effectively isolated from sword (Xiphias gladius) and tuna (Thunnus thynnus) fish bones through thermal treatment at 900 °C, as described in reference [1]. demonstrated that HA derived from micropogonias furnieri (whitemouth croacker) fish refuse and calcined at 800 °C has great potential as a biomaterial owing to its low cost, simple production, and high biocompatibility. Nevertheless, knowledge remains limited and discoveries pertaining to them are in contrast to those concerning alternative biological sources. HA extraction from the untapped biowaste of carp fish bones is the objective of this research. XRD, FTIR, and FSEM were employed to characterize the material. In order to establish bioactivity in vitro, dissolution and bioactivity assessments were conducted over a period of 14 days at 37 °C using synthetic body fluid (SBF).

## 1. 10 future perspectives

The most recent data regarding the utilization of hydroxyapatite as a clipper in fabric control pertains to investigations concerning its physical-chemical properties and organic reaction. The results of this study suggest that [82], which supports cellular proliferation in vitro, are accompanied by a reduced risk of transmitting pathogens and outstanding biocompatibility [83]. Consequently, hydroxyapatite for snapper is a potentially valuable byproduct of industrial application, textile manufacturing, and medical and dental products. Nonetheless, numerous obstacles and constraints must be surmounted in order to implement it. The evaluation of biocompatibility must be conducted through in vitro and in vivo investigations involving distinct species of fish; this is a viable approach to ascertain the fabric's ability and security. In addition, distinct documentation must be implemented and examined during the display of hydroxyapatite of Pisces. Recent studies have validated the feasibility of fabricating nano-sized hydroxyapatite pigeonhole imitators with larger dimensions. the substances added to bone tissue [84].

## 1.11 Thermal calcination method of HA

Recent research has focused on the utilization of hydroxyapatite in the texture facet of pouter, particularly in relation to its physical-chemical properties and natural reaction. These results support that [82], which promotes cellular proliferation in vitro while posing little risk of transport from contaminants and ensuring excellent biocompatibility [83]. Within the given framework, hydroxyapatite of gudgeon serves as a valuable resource at high altitudes, particularly for industrial applications and as a component of medical and dental

products. Nevertheless, certain limitations must be surmounted. All biocompatibility assessments must be conducted using in vitro and in vivo studies, with the employment of particular fish species serving as an effective method to evaluate the fabric's safety and performance. Moreover, when exhibiting HA derived from fish, specific documentation must be synthetic and tested. Innovative research has demonstrated [84]. As a result, nano-HA fish-based fully biomaterials have the potential to provide HA, exhibiting enhanced bioactivity during degradation compared to irregular crystals due to their high floor-to-area ratio and specific chemical properties [85]. As a result, the potential purchase of nano-hydroxyapatite from Pisces may result in increased osteoblast adhesion and mobile proliferation [86]. The increased consumption of pouter in the industry has led to a significant increase in the disposal the waste of fish in the shape of scales. The process of recovering fish scales and bones yields parent HA and recoups substantial residues generated during the fisheries industry [91]. Fish bone is an exceptionally abundant resource for the extraction of HA. The morphological dissection of the HA, which was obtained for the mammalian loftiness display, reveals that the detritus is predominantly asymmetrical in shape, with variations observed in the final complexion morphologies across different research performances. The shape version is therefore not considered to be affected by the approach or fountain. For instance, a model calcification of an identical supply of loftiness has the potential to generate various morphologies of HA [98]. In the same way that specific extraction techniques, such as alkaline hydrolysis, can produce HA in the form of rods, there may be no correlation between the morphology of HA and its supply or descent procedure [7]. The obtained HA dimensions exhibited no discernible correlation with the extraction method.

Supplemental milling was utilized to minimize the volume of the HA particle to a nanometer scale, which is comparable in length to human being HA [99]. Additional floor action and ultrafine systems that are increasing [100].

## 1.12 Opportunity preparation approach

Resesrchers have undertaken investigations into the production of calcium phosphates for standby purposes, employing techniques like alkaline hydrolysis, hydrothermal, and laser ablation. HA was utilized to collect an assemblage of red shark. Pisces loftiness-based completely macroscale detritus through the use of a laser ablation device formulated for compressed petrol plane without prior calcification [101]. The investigation validated the feasibility of extracting calcium phosphates through direct ablation without the need for calcination. The process of instruction was examined [92]. Fish bones underwent a preliminary calcination process at 100 °C to remove any organic contamination, followed by milling to obtain particles on the microscale. Hydroxyapatite microparticles were employed as starting material in laser-induced fragmentation analyses. Particles of β-TCP and hydroxyapatite measuring 10 nm in diameter were received in nanometric form. Boutinguiza et al. [102] have utilized $CO_2$ throb laser ablation in all other investigations to obtain calcium phosphate nanoparticles from swordfish bones that were previously calcined at 600 °C. approximately 25 nm in diameter at the median [103].

## 1.13 Dicalcium Phosphate (DCP) Cements

Monetite and Brushite Almost two decades have passed since the invention of dicalcium phosphate cements. Since then, considerable research has been conducted to enhance the properties of dicalcium phosphate cements for clinical applications and to meet the requirements. Dicalcium phosphate anhydrous (DCPA) and dicalcium phosphate dihydrate (DCPD) are the two classifications of DCP cements.

## 1.14 Brushite and Monetite Cement, Structure and Properties

Dicalcium phosphate cements have demonstrated efficacy from animal models for bone regeneration in various orthopedic sites, including condyle, distal femoral metaphysis, and epiphysis [105]. In 1989, brushite cement was discovered by Mirtchi and Lemaitre [106] through the combination of β-TCP, water, and MCPM. The resulting blend was a flexible adhesive that harden through an exothermic reaction, producing a substance composed of DCPD, also known as "brushite" $CaHPO_4.2H_2O$ [106].

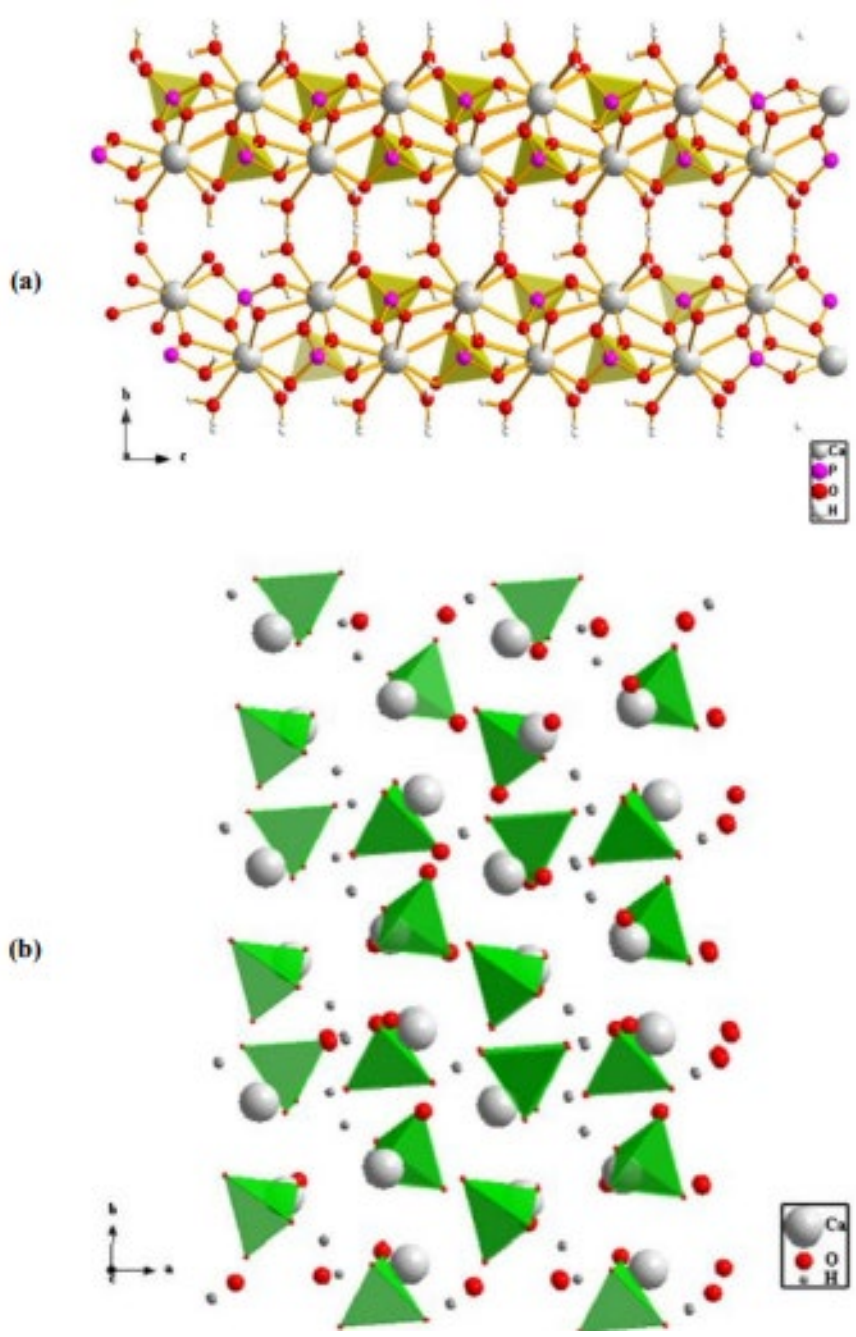


**Figure 1.4** Projection view of (a) brushite and (b) monetite

Subsequent research has provided evidence that brushite cement is biocompatible and capable of undergoing reabsorption under physiological conditions. The

principal components of dicalcium phosphate (DCP) cement are an acidic phosphate source, water, and an antacid calcium precursor. However, additional substances may be incorporated into the mixture to extend the setting time, improve mechanical properties, or facilitate bond treatment. Brushite (DCPD) bonds serve as precursors to monetite (DCPA), also known as anhydrous DCP. The exothermic precipitation of brushite is commonly facilitated by the setting of DCP bonds [108]. The crystal structure of brushite is monoclinic (space group Ia). As illustrated in Figure 1.4 (a), the unit cell of brushite contains four $CaHPO_4 \cdot 2H_2O$ motifs. The latter indicates that the crystals consist of brushite corrugated sheets with a $CaHPO_4$ composition. These sheets are aligned parallel to one another, with a direction perpendicular to axis b. A double layer of water molecules connects the sheets [107]. In animal models, DCPs have been tested and found to be effective for bone regeneration at various surgical sites, including the condyle, epiphysis, and distal femoral metaphysis [105]. In 1989, Mirtchi and Lemaitre discovered brushite cements through the combination of water and a powdered compound consisting of β-tricalcium phosphate and an acidic calcium phosphate (monocalcium phosphate monohydrate). The resulting mixture was a flexible adhesive that eventually solidified in an exothermic reaction, forming a rigid substance composed of DCPD, also known as "brushite" [106].

## 1.15 Setting Time of bone cement

The setting time is a critical factor in meeting clinical requirements; prolonged setting times can lead to clinical complications because cement is unable to retain its shape and withstand stresses during this period. [114]. Following the combination of solid and liquid phases during the formation of bone cement, a setting reaction occurs, resulting in the formation of cement. The setting reaction of DCPD depend of the following: (i) dissolution of cement particle constituent in a solvent; (ii) consistence of a supersaturated gel; (iii) nucleation within the gel; and (iv) formation of interlocked crystals that compose the solid. The setting reaction of the β-TCP/MCPM bonds initiates with the dissolution of MCPM, which rapidly results in a decrease in pH to 2.5 [115,116]. An overabundance of MCPM results in the cement maintaining a low pH even after the curing reaction has concluded. In contrast, when the quantity of β-TCP is substantial, the bond's pH equals 5 [117]. Vicat needles or Gilmore needles are utilized to verify that the cement has completely hardened [5,118]. A macroscopically solid cement is typically characterized by the absence of discernible penetration of the needle into the cement surface. The international standard (ASTM C266-89) specifies that the ultimate setting of the β-TCP/MCPM cement framework occurs shortly after blending [119]. For particular applications, the optimal value of the setting time is contingent on the surgical procedures involved. Surgeons recommend an initial setting time of 3 to 8 minutes, with approximately 8 minutes designated for orthopedic procedures and 3 minutes for dental procedures [120]. For both applications, an ultimate setting time of less than 15 minutes is preferable.

## 1.16 Injectability

Vessel Injectability The injectability of the cement is critical for minimally invasive surgery involving the injection of the cement into a bone defect [121]. The cement's injectability is restricted as a result of the solid phase and liquid phase being separated via filter compression [18]. The limited injectability of various brushite formulations can be attributed to a phase separation issue. The mechanisms of phase separation that are observed during the excursion of cement paste. To address these challenges, one may consider increasing the extrusion speed and utilizing a shortened canula syringe, both of which have been observed to enhance injectability [74]. Additionally, the injectability of cement can be enhanced through the following methods: rising the viscosity of the mixing liquid, decreasing the PLR, conducting extensive processing of the cement powder, utilizing modified cement reagents to decrease the particle–particle interface, and adding carboxylic acids as additives [18,121]. Doping β-TCP with Mg, Sr, and Si ions has been observed to enhance the injectability of DCP cement [11, 13, 14, 122]. This effect of increased injectability cannot be generalized, as doping -TCP with Sr ions has also been reported to decrease the injectability of the cement [11]. Additional significant characteristics of DCP cement may be subject to alteration as a result of efforts to improve injectability. Likewise, a reduction in PLR results in compromised mechanical characteristics of the cement [123]. Due to the paste-like consistency that results from combining polymeric materials such as chitosan, alginate, and gelatine into CPCs, their handling properties can also be enhanced [114].

## 1.17 Mechanical Properties

The only criterion frequently used to evaluate the mechanical performance of CPCs is their compressive strength [3]. This criterion is frequently employed to estimate the mechanical performance of CPCs. In general, the compressive strength of apatite CPCs is higher than that of brushite CPCs [3]. bio ceramics and cement designed for regeneration of bone should possess the same mechanical properties as bone. Pure brushite cement, however, as Lemaitre and Mirtchi have prepared it, possesses weak mechanical properties. A variety of approaches (including the incorporation of polymers and ions such as $Mg^{2+}$, $Sr^{2+}$, $Zn^{2+}$, among others) have been explored in order to tackle this issue [106,124]. Prior to testing, brushite cements are commonly allowed to harden for a minimum of 24 hours so that their mechanical properties can be evaluated (ISO 5833, 2002) [3,125]. CPC it may maintained under physiological conditions (37 °C and 100% humidity) or dry conditions (room temperature and humidity) throughout the setting time [126]. Clinically pertinent data is collected during the storage of CPC specimens under physiological conditions. As a means of determining whether a cement is suitable for biomedical applications, its compressive and tensile strengths are typically evaluated [5]. In contrast, the porosity of brushite cements is correlated with their compressive strength [125,126]. Reducing the porosity of the cement results in enhanced mechanical performance. By compacting the CPC during the setting reaction, its porosity is decreased, which increases the bone cement's compressive strength [127]. By optimizing the setting response conditions, cement systems that expend water through the setting, such as DCPD, could theoretically product ceramics without porosity. This was achieved through the augmentation of PLR proportion and the incorporation of setting retardants, which impede the ascent of

crystals [126]. To development the mechanical properties of DCP that can be doping of (Mg, Sr, Zr, and Si) may be employ [125,128]. The introduction of ions as free into a cement typically an influence on the setting time of the cement, but does not typically improve its mechanical properties. The introduction of metallic ions in the form of chloride compounds (e.g., $SrCl_2$) into cement during the setting reaction does not yield favorable results in terms of influencing the mechanical properties of the cement [129]. 32 Presumably, this occurs due to the formation of a soluble sodium chloride at cement, which compromises structural integrity. On the contrary, the introduction of ions as an alternative to phosphate or calcium enables the formation of phases that are less soluble, thereby contributing to the improvement of the cement's mechanical properties. For instance, the addition of Sr ions to cements can produce at 20% increase in the compressive strength of CPC based on β-TCP [11,130,131]. The compressive strength of pure brushite cements can be increased by as much as 40 MPa with the inclusion of magnesium. [132].

## 1.18 Antibiotics

Significant observation devoted to antibiotics due to their wide-ranging applications, including prophylactic measures to prevent surgical-associated infections and preferred treatments for bone infections [104]. In reality, a single determinant for the success of surgical procedures involving the insertion prosthesis at prohibition of contagion [105]. Developed complications may arise as a result of wound infection, postoperative infections following vertebral column surgical procedure, combined prosthesis insertion, or fracture restoration [106]. Due to this, prophylactic antibiotics are frequently administered orally or

intravenously. Conversely, the moderate susceptibility of the site of infection to antibiotics administered systemically extends the treatment duration of bone infections by an average of one year [107].

In order to mitigate the occurrence of plant-associated infections, a multitude of external biomaterial interventions have been suggested. Previous research aimed to imbue biomaterials with antibacterial properties through roof functionalization techniques, such as coating cultivate surfaces with silver ions. [108].

## 1.19 Problem Statements

The majority of traditional chemical processes utilize HA synthesis without introducing any trace amounts of beneficial elements, including $Na^{+}$, $Zn^{2+}$, $Mg^{2+}$, $K^{+}$, $Si^{+}$, $Ba^{2+}$, $F^{-}$, $CO_3^{2-}$, and others. The inclusion of these ions has a direct impact on a range of biochemical reactions associated with bone metabolism. Despite the existence of numerous synthesis methods, the production of HA with specific properties continues to be a formidable task due to the potential formation of hazardous intermediate products. As a result, research into additional HA synthesis parameters remains ongoing. It is possible to chemically synthesis HA or extract it from natural sources. HA and its antecedents are extracted from natural biological reservoirs that are economical to obtain, such as the bones of mammals and fish.

Due to their high calcium, phosphate, and carbonate content, fish and bovine bone are excellent sources for HA extraction. Carbonate, phosphate, and calcium, all of which are abundant in fish bones, can be utilized in the production of HA. The synthesis of these bioactive compounds can be achieved through various straightforward methods. In general, calcium is extracted from fish bones for use in dietary products;

nevertheless, biomedical applications of HA synthesized from these natural sources have received scant attention. DCPs are frequently favored in orthopedic procedures over alternative calcium phosphate-based biomaterials. Present approaches to the development of CPCs are centered on enhancing the cements' in-situ setting characteristics while maintaining satisfactory mechanical properties under physiological conditions.

Brushite and monetite cement's rapid setting time has restricted their clinical applications. In addition, injectability is typically subpar in DCP cements that do not contain any added substances due to the liquid–solid stage separation. The presence of specific ions within the cement has the potential to influence the setting response, which in turn can affect the setting time and ultimate properties of the cement. Without additives, DCP cements typically have weak injectability as a result of the separation of the liquid and solid phases. The initial and final setting time properties of cement can be influenced by the setting reaction, which can be affected by the presence of specific ions in the cement. In minimally invasive surgical procedures, cement injectability is critical, as it permits the cement to be injected into bone defects. However, when it comes to surgical interventions involving the implantation of prostheses or osteoconductive materials, preventing bacterial infections or postoperative infections after fracture repair are critical success factors. Such infections can lead to severe complications. The advantage of employing antimicrobial agents, such as antibiotics, is that they inhibit the growth of resistant microorganisms and are rapidly eliminated by body fluids; thus, they can prevent post-operative infections for an extended period of time. By utilizing biomaterials that encapsulate antimicrobial agents, which are gradually eliminated by bodily fluids, it is possible to avert post-surgical infections gradually.

## 1.20 Objectives of the Study

1. To study investigates the impact of natural waste source and extraction process on critical HA properties, including particle diameters, morphology, crystallinity, and phase assemblage.

2. To highlight the significance of HA extraction from natural resources and provides the researcher with future directions to enable the clinical application of HA extracted from biological resources as a valuable biomaterial.

3. To produce dicalcium phosphate cements through the Preparation of the corresponding HA precursors.

4. To evaluate the mechanical properties, injectability, and setting time of dicalcium phosphate cements.

5. To determine whether dicalcium phosphate cements have the capacity to serve as drug carriers in applications requiring sustained drug release.

.

## 1.21 Significance / Novelty of the study

This research endeavors to produce HA synthetically from natural sources. The primary aim of our research was to identify a feasible source within our nation for the extraction of HA. The aim of this research was to determine the composition and properties of natural HA derived from sources that were subjected to a high-temperature (900°C) treatment. 1.67 was determined to be the Ca/P molar ratio, which corresponds to the stoichiometries of HA. As a biomaterial, these findings possess potential for use in biomedical applications. The materials extracted in this study represent a modest endeavor to manufacture bioactive substances in Iraq, thereby substantially decreasing their price and rendering them accessible to the general populace at an affordable cost. This investigation will yield significant insights in addition to elucidating the physicochemical characteristics of DCPD. When attempting to predict the in vivo efficacy of these materials for bone repair, these properties are crucial.

# CHAPTER TWO

# METHODOLOGIES

## 2.1 Introduction

This chapter outlines the comprehensive methodology employed to extract HA from marine fish (LN) (Lethrinus Nebulosus, Forsskal 1775) (spangled emperor, FAO), bovine bone (BB) procured from a market in Misan, Iraq, and Diagramma pictum (DP) procured from a market in Basrah, south Iraq (Thunberg, 1792). The procedure for preparing cement. Chemicals of the reagent grade are utilized in the fabrication of synthetic body fluid (SBF) and bone cement. In addition, procedures for measuring setting time, injectability, compressive strength, and in vitro ion release experiments in SBF are detailed in this chapter. Raw bone is depicted in figure 2.1, while figure 2.2 illustrates the stages of HA extraction and cement preparation.

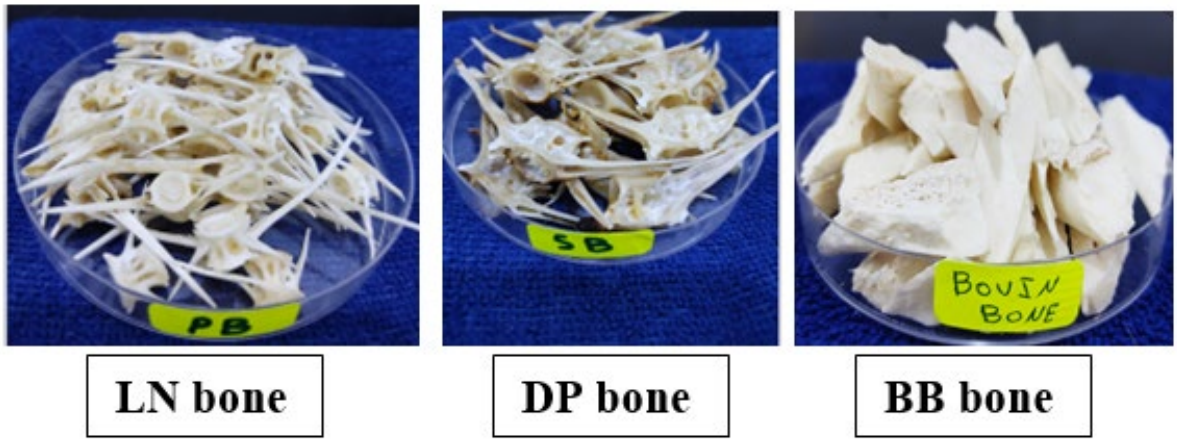


**Figure 2.1:** Raw bone

## 2.2 Materials and Chemicals

Every chemical utilized in the synthesis process was of reagent grade and was employed exactly as it was received.

In order to assess the in vitro bioactivity, simulated body fluid (SBF) was prepared in accordance with the methodology outlined in (Kokubo 1990) (Table 2.1). The preparation of simulated body fluid (SBF) solution followed methodologies that have been previously documented. In particular, HCl was added to a solution comprising NaCl, $CaCl_2$, $NaHCO_3$, KCl, $K_2HPO_4$ and $Na_2SO_4$, and as a liquid in order to achieve a pH value of 7.4. Our specimen was submerged in 20 mL of SBF solution via a 37°C water path.

**Table 2.1:** Ionic composition of SBF and human blood plasma

| Ions | pH* | $Na^+$ | $K^+$ | $Ca^{2+}$ | $Mg^{2+}$ | $Cl^-$ | $HCO_3^{3-}$ | $HPO_4^{2-}$ | $SO_4^{2-}$ |
|---|---|---|---|---|---|---|---|---|---|
| **SBF (mM)** | 7.4 | 142.0 | 5.0 | 2.5 | 1.5 | 147.8 | 4.2 | 1.0 | 0.5 |
| **plasma(mM)** | 7-7.4 | 142.0 | 5.0 | 2.5 | 1.5 | 103.0 | 27.0 | 1.0 | 0.5 |

*The pH of SBF is adjusted by using tris-hydroxy methylamino methane $(CH_2OH)_3CNH_2$) buffer solution and 1M HCl.

All chemicals that are used to prepare SBF are purchased from (QREC, Auckland, New Zealand).

### 2.2.1 Equipment and Apparatus

In this study. The following apparatus and equipment were used.

**Table 2.2.** Apparatus used during the study period with the name of the Manufacturer and the country of Origin

| NO. | Equipment and apparatus | Company \ origin | place |
|---|---|---|---|
| 1 | X-Ray Diffraction (XRD) | Philips PW1730 | Tehran/ Iraq |
| 2 | FTIR spectrophotometer (spectrometer) | Nicolet iS50 | BPC Analysis Center Adhamiya/Baghdad |
| 3 | Field Emission Scanning Electron Microscope (FESEM) | Zeiss-LEOModel1530 | Tehran University/Advanced Materials Characterization Instityte |
| 4 | X-Ray Analysis Energy Dispersive | Zeiss-LEOModel1530 | Tehran/ Iraq |
| 5 | UV-Vis Spectroscopy | UV-3101PC; | BPC Analysis Center Adhamiya/Baghdad |
| 6 | Flame atomic absorption spectroscopy, Al 1200 | (Perkin Elmer A Analyst 400). | BPC Analysis Center Adhamiya/Baghdad |
| 7 | Gilmore needle apparatus (ASTM C266) | | National University of Singapore /Singapore |
| 8 | 2.5 T Universal Testing machine by INSTRON | Singapore | National University of Singapore /Singapore |

### 2.2.2 Chemicals

**Table 2.3**. All Chemicals Used in the study with the Name of the Company Manufacturer and Country of Origin.

| NO. | Chemicals | Company/origin |
|---|---|---|
| 1 | Aceton | Sigma Aldrich |
| 2 | Petroleum ether | Sigma Aldrich |
| 3 | Potassium chloride | QREC, Auckland, New Zealand |
| 4 | Sodium chloride | Sigma Aldrich |
| 5 | Potassium chloride | Sigma Aldrich |
| 6 | Sodium hydrogen carbonate | Sigma Aldrich |
| 7 | Potassium phosphate | QREC, Auckland, New Zealand |
| 8 | Magnesium di chloride | Sigma Aldrich |
| 9 | Hydrochloric acid | Sigma Aldrich |
| 10 | Calcium chloride | Sigma Aldrich |
| 11 | Sodium sulfate | QREC, Auckland, New Zealand |
| 12 | Trisodium citrate | Sigma Aldrich |

## 2.3 Samples Preparation

The calcination process was employed to extract HA from bone powder prepared from bovine bone. The modified procedures by which bone samples were cleansed with a keen knife to remove visible impurities were utilized to extract HA. Small sections were extracted by employing a hacksaw. In a sealed container, the pieces were simmered for approximately two hours to eliminate macroscopic adhering impurities. Following several washes with distilled water, the samples were immersed in a solution of acetone and ether in a 3:1 ratio for 24 hours in order to

eliminate the invisible fat. To prevent the formation of shoots during the milling process, the samples were desiccated in a heated air oven at 120°C for 17 hours. Utilizing an iron mortar and pestle, dehydrated bone samples were pulverized into granules measuring a range of 0.2 mm in particle size.

The calcination procedure was executed, during which the unprocessed material was subjected to furnace heating at a rate of 5 °C/min for 5 hours at temperatures varying from 200 °C,700 and 900 °C. HA was extracted from fish using the calcination method for a duration of 2 hours calcination at 200 °C, 700 °C, and 900 °C. For extraction of HA from fish (LN) (Lethrinus Nebulosus, Forsskal 1775) (spangled emperor, FAO), and (DP) Diagramma pictum (Thunberg, 1792) specimens were prepared according to the identical methodology as that employed for bovine bone.

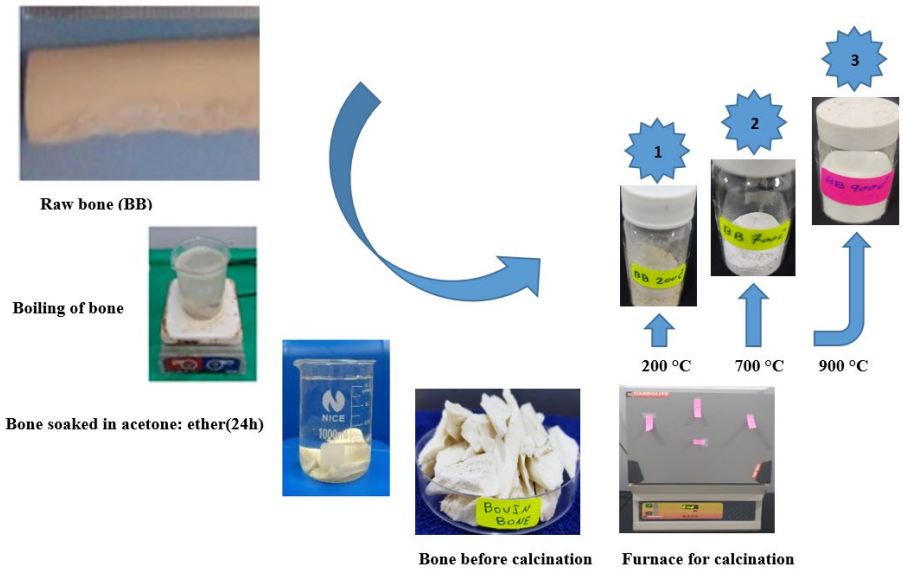


**Figure 2.2:** Stages of extracted HA

**Figure 2.3**: Appearance of bone powder after heat treatment at 200, 700 and 900 °C.

## 2.4 Preparation of Dicalcium Phosphate Dihydrate (DCPD) Cement

In a mortar and pestle, HA extracted from bones and monocalcium phosphate monohydrate (MCPM) (MW 252.07, Sigma Aldrich (USA)) were combined to produce a particle known as the solid phase for cement preparation. For the preparation of DCPD cement, solid and liquid phases were combined in varying proportions of granules to liquid. The ingredients were combined through mixing until a uniform substance was formed. The material quantities utilized for the various PLRs are detailed in Table 2.4. After combining the solid and liquid phases by hand in a mortar for approximately one minute, the resulting material was transferred into cylindrical Teflon molds with dimensions of (D = 6mm × h= 12 mm). These molds were subsequently utilized to determine the setting time utilizing a Gilmore needle. Visual representations of the cement preparation process are presented in Figure 2.4.

**Table 2.4**: Deferent ratio of solid and liquid phases

| Sample ID | Solid phase | Liquid phase |
|---|---|---|
| | MCPM/HA (gm) | Trisodium citrate(ml) |
| 1 | 4:1 | 1ml (1M) |
| 2 | 1:4 | 1ml (0.25M) |
| 3 | 2:2 | 1ml (0.5M) |
| 4 | 1:4 | 0.5ml (0.1M) |
| 5 | 1:2 | 0.5ml (0.1M) |

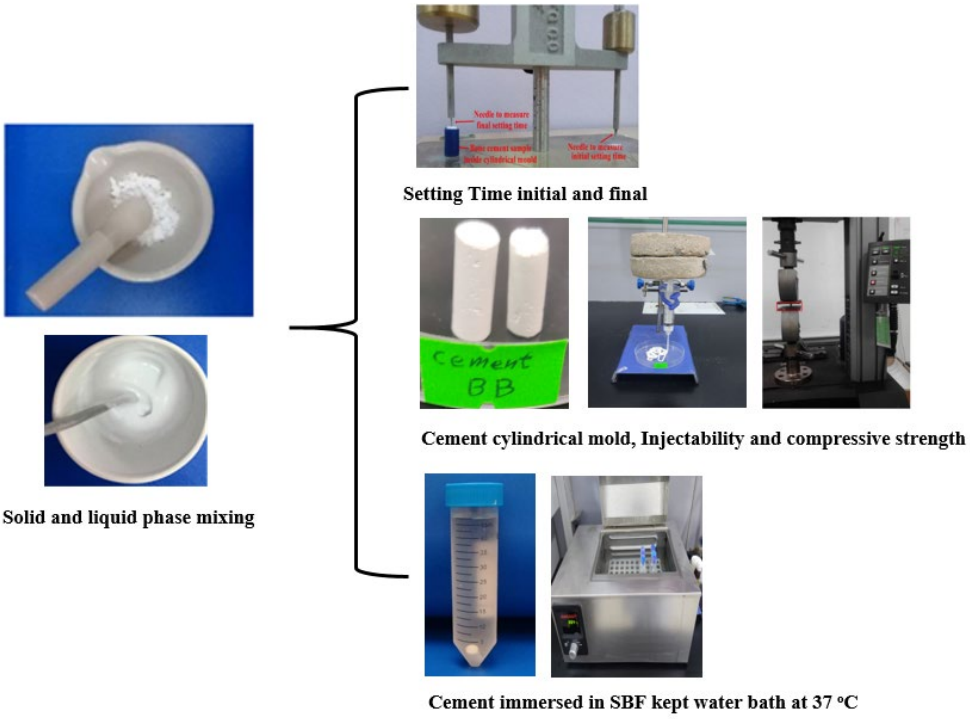


**Figure 2.4**: Preparation of cement

## 2.5 Setting Time Measurement

The Gilmore needle apparatus (ASTM C266) was utilized to determine the initial and ultimate setting durations of the prepared cement samples, as illustrated in figure 3.4. Cement material was deposited into a cylindrical Teflon mound with a dimension of 6mm × 12mm. A needle with a diameter of 2.12 mm and a mass of 113.4 g was positioned atop the specimen. Initial setting time was determined as the moment this needle etched the surface of the cement sample without leaving any indentations. Similarly, an additional needle with a diameter of 453.6 mm and a mass of 1.06 g was employed to measure the ultimate setting time [4]. In conclusion, the mean values of three measurements were utilized to record the initial and final configuration durations for each distinct PLR.

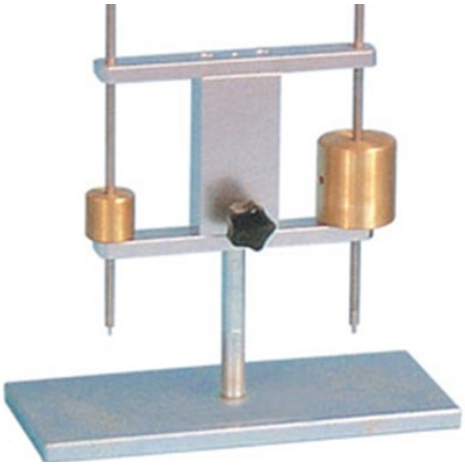

**Figure 2.5:** Gillmore needle for measurement of setting times

## 2.6 Injectability Measurement

A 2:1 DCP powder to liquid (P/L) ratio is manually combined for two minutes in order to achieve a uniform paste. The homogenized material is introduced into a commercial hypodermic featuring a 2 mm opening in the cartridge, which has a nominal capacity of 10 ml and a diameter of 13 mm. Then, for two minutes, a 5 kg compressive weight is vertically affixed on the highest point of the plunger. A series of injections are performed until the mixture becomes entirely unsuitable for injection Figure 2.4. In order to determine the percentage of injectability, one applies Equation [240 A].

$$\mathbf{Inj\% = W_F - W_A / W_F - W_E \times 100}$$

Where Inj% is the percentage injectability, $W_E$ are the weight of the empty syringe, $W_F$ is the weight of the syringe full of paste and $W_A$ is the weight of the syringe after the injection.

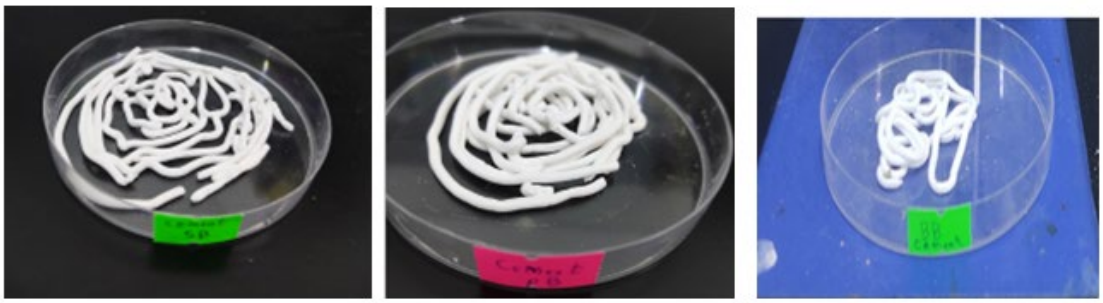


**Figure 2.6:** Injectability of cements

## 2.7 Tests of compressive strength

Circular specimens of DCPD were fabricated using a plastic cylindrical with the following dimensions: 6 mm in diameter and 12 mm in height. For 1, 3, and 7 days, the samples were submerged in solution of SBF. In accordance with ASTM F451-99a [241 A], the cemented samples were extracted from the mold and meticulously polished with SiC sandpaper of 800 grains to reach a height of 12 mm on the extremities. The specimen's compressive strength was determined using an 2.5 T Universal Testing machine by Instron with a crosshead speed of 0.5 mm/min after a 24-hour drying period at room temperature (Figure 2.4). The value of compressive strength is calculated by averaging five values.


**Figure 2.7:** 2.5 T Universal Testing machine by INSTRON.

## 2.8 Determination of ions release

In order to assess the ion release characteristics of DCP cement samples, the cement material was deposited into cylindrical Teflon molds with a height of 12 mm and a diameter of 6.0 mm. Following synthesis, specimen was left at 25 °C for 24 hours. Submerging samples set in SBF solution. The concentration and chemical composition of the SBF solution resembled those of the inorganic component. It was prepared by dissolving reagents as in Table 2.1which deionized water per Kokubo's specification. Hydrochloric acid, HCl, was used to adjust the pH of the solution to 7.25. The samples were stored in SBF at 37 degrees Celsius for increments of one, three, and seven days. Following that, the complete volume of the SBF was extracted in order to quantify its $Ca^{2+}$ concentration, and subsequently re-fed with fresh solution. The concentrations of $Ca^{2+}$ were ascertained utilizing a FAAS.

## 2.9 *In vitro* determination release of drug profiles

In order to prepare samples for the assessment of in vitro antibiotic release from the DCPD, DCPD-containing antibiotic is positioned. Following preparation, samples are allowed to rest at ambient temperature for 24 hours. Three specimens are submerged in 15 ml of SBF from each batch in water bath at 37 °C ± 0.5 °C. 2 ml of the solution is extracted the receptacles at the following time intervals: 30 minutes, 1 hour, 2 hours, 3 hours, 4 hours, 5 days, 6 days, 7 hours, 12 hours, 24 hours, 48 hours, 72 hours, and 186 hours. A comparison is made between the quantity of antibiotic released and a calibration curve that is specific to the antibiotic produced in SBF. The quantification of antibiotic concentration in

dissolution medium is accomplished through the utilization of ultraviolet–visible spectroscopy.

## 2.10 Characterization

### 2.10.1 X-Ray Diffraction (XRD)

The crystallinity and phase integrity of each sample were assessed using an X-Ray Diffractometer (XRD, Bruker D8) set at 30 mA and 40 kV, employing CuKα radiation. The diffractograms were recorded at 2θ angles ranging from 20° to 80° with a step size of 0.02° and a time interval of 1 second.

The degree of crystallinity was determined by utilizing X-ray diffraction data to determine the proportion of crystalline phase present in the volume under analysis.

$$X_C = 1 - (V_{112/300} / I_{300}) \times 100\% \quad \textbf{(}\text{Equation 3.1}\textbf{)}$$

where $X_C$ is the degree of crystallinity, $I_{300}$ is the intensity of (3 0 0) reflection and $V_{112/300}$ is the intensity of the hollow between (112) and (300) reflections.The average crystallite size was calculated using Scherrer's equation

$D = 0.9\lambda/\beta\cos\theta$, (Equation 3.2)

where $D$ = crystallite size (nm), $\lambda$ = wavelength of the X-ray used (nm), $\beta$ = full width of the line at half of its maximum intensity in radians (FWHM),

$\theta$ = diffraction angle

For crystallite size calculations we used the FWHM at (002), (300), (222) and (310) reflections.

Calculation of lattice parameters *a*, *c* and cell volume (*V*) of ion substituted CaP structure were made using the unit-cell program of Holland and Redfern. The percentage presence of secondary phase in the samples was determined from relative intensity ratio of the corresponding major phases by using (Equation 3.3a, b)

Presence of phase to be determined = Relative Intensity ratio of the phase x 100 (Equation 3.3a**)**

Relative Intensity ratio = Intensity of the major peak of the phase / ∑ Intensity of major peaks of all phases (Equation 3.3b**)**

## 2.10.2 Fourier Transform Infrared Spectroscopy (FTIR)

The KBr disc method was employed to corroborate the presence of functional groups using an FTIR spectroscopy (Nicolet iS50 spectrometer). All spectra were acquired in transmission mode, covering the scanning range of 4000-400 $cm^{-1}$.

## 2.10.3 Field Emission Scanning Electron Microscope (FESEM)

The morphology and microstructure of the DCPD and HA were analyzed using a FESEM (Zeiss-LEOModel1530) coupled to an (EDX) system operating at a potential of 20 Kv. Prior to analysis, samples were gold or platinum-coated to prevent charge accumulation. Utilizing an EDX capable of operating at 15 kV of voltage, the elemental composition of the apatite layer that formed when samples were submerged in SBF was analyzed. To compute the average elemental composition, measurements were taken at five distinct locations.

### 2.10.4 UV-Vis Spectroscopy

On a Shimadzu 3101 UV-Vis-NIR spectroscopy, the absorption spectra of antibiotic release from DCPD-loaded antibiotic samples are recorded within the 200-800 nm spectral range.

Utilizing a twofold monochromatic diffraction grinding framework and a photomultiplier R-928 indicator with a resolution of approximately 0.1 nm, the absorbance is determined.

# CHAPTER THREE

# RESULTS AND DISCUSSION

## 3. Extracted Hydroxyapatite (HA) from different sources (different animals)

Hydroxyapatite (HA) is obtained through a two-hours calcination process at 900°C from bone various sources (including animals). In order to ensure consistent testing, three distinct varieties of HA are produced by calcining bones obtained using an identical procedure. Table 3.1 provides a description of the HA samples that were extracted from three distinct forms of bone.

**Table 3.1** Description of HA samples extracted from different sources

| Sample | Description |
|---|---|
| BB | HA extracted from bovine bone |
| LN | HA extracted from fish (Lethrinus Nebulosus, Forsskal 1775) (spangled emperor, FAO) |
| DP | HA extracted from fish (Diagramma pictum (Thunberg, 1792) |

## 3.1 Extraction of Hydroxyapatite (HA) from bovine bone (BB)

By means of calcination, HA was extracted from bovine bone (BB) sourced from Misan, located in southern Iraq. The bone powder underwent calcination; the unprocessed powder was heated in a furnace to calcination two hours at of 200 °C, 700 °C, and 900 °C at a rate of five degrees Celsius per minute. HA was extracted from (BB) via calcination at 200 °C, 700, and 900 °C for a duration of two hours.

### 3.1.1 X-Ray Diffraction (XRD) Analysis

XRD was utilized to analyses the structure of bovine bone (BB) powder at various temperatures (figure 3.1). The phase analysis of size-controlled HA is evaluated in comparison to the ICDD (International Centre for Diffraction Data standard HA) PDF card no. 00-009-0432. The comparison reveals that the principal diffraction peaks at 2θ values of 33.424°, 34.165°, 40.722°, 46.954°, and 52.271°, which correspond to the Miller Indicies (310), (222), (213) and (002), respectively, are in satisfactory agreement with the standard HA [3]. The lattice parameters of the hexagonal structure of HA are as follows: a = b = 9.416A°; c = 6.863 A°; and cell volume = 527.3 (refer to Table 3.2). The outcome of the XRD analysis performed in the current study is highly consistent with the results that have been previously reported[4].

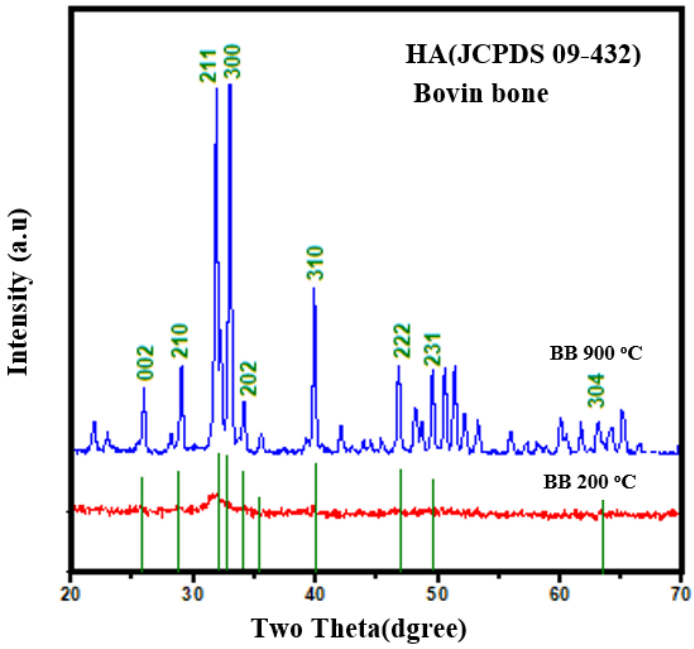


**Figure 3.1**: XRD pattern of HA calcined at 200 and 900°C for 2 h.

**Table 3.2:** Lattice parameters of HA from bovine bone (BB) calcined at 900 °C plus degree of crystallinity.

| Samples | Chemical formula | Lattice Parameter | | | $X_c$ | *D* |
|---|---|---|---|---|---|---|
| | $Ca_{10}(PO_4)_6(OH)_2$ | *a* (Å) | *c* (Å) | *V* (Å)$^3$ | (%) | (nm) |
| Standard HA | $Ca_5(PO_4)_3(OH)$ | 9.418 | 6.884 | 528.8 | ---- | ---- |
| HA (900) | $Ca_{10}(PO_4)_6(OH)_2$ | 9.418 | 6.866 | 527.4 | 86 | 98.23 |

## 3.1.2 FTIR spectra analysis

The FTIR spectra of chicken bone calcinated at two distinct temperatures (200°C and 900°C) are illustrated in Figure 3.2. The dissimilarities in spectra between untreated and heated chicken bones are evident, as illustrated in Figure 3.2, as a result of the modifications that occur in their chemical bonds during the process of heat treatment. The coloration of bone particles undergoes a discernible transformation from yellowish white to white subsequent to calcination.

Through FTIR spectra, it is also revealed the presence of phosphate ($PO_4^{3-}$), and hydroxyl ($OH^-$) groups. These spectra are more clearly appeared in calcinated samples because the calcination process has destroyed the cross-linked structure in the BB bone. ($\nu_4$) ($PO_4^{3-}$) group were recorded at 520 $cm^{-1}$, ($PO_4^{3-}$ ($\nu_2$), 480 $cm^{-1}$ $PO_4^{3-}$ ($\nu_2$), 530 $cm^{-1}$ ($PO_4^{3-}$ ($\nu_4$), and 980-1200 $cm^{-1}$ ($PO_4^{3-}$ ($\nu$1,3). The stretching and bending mode of hydroxyl (OH) group were observed at 3566 $cm^{-1}$ The sharp narrow band at wide band at 3572 $cm^{-1}$ are associated with hydroxyl group where these peaks prove the presence of HA phase [4].

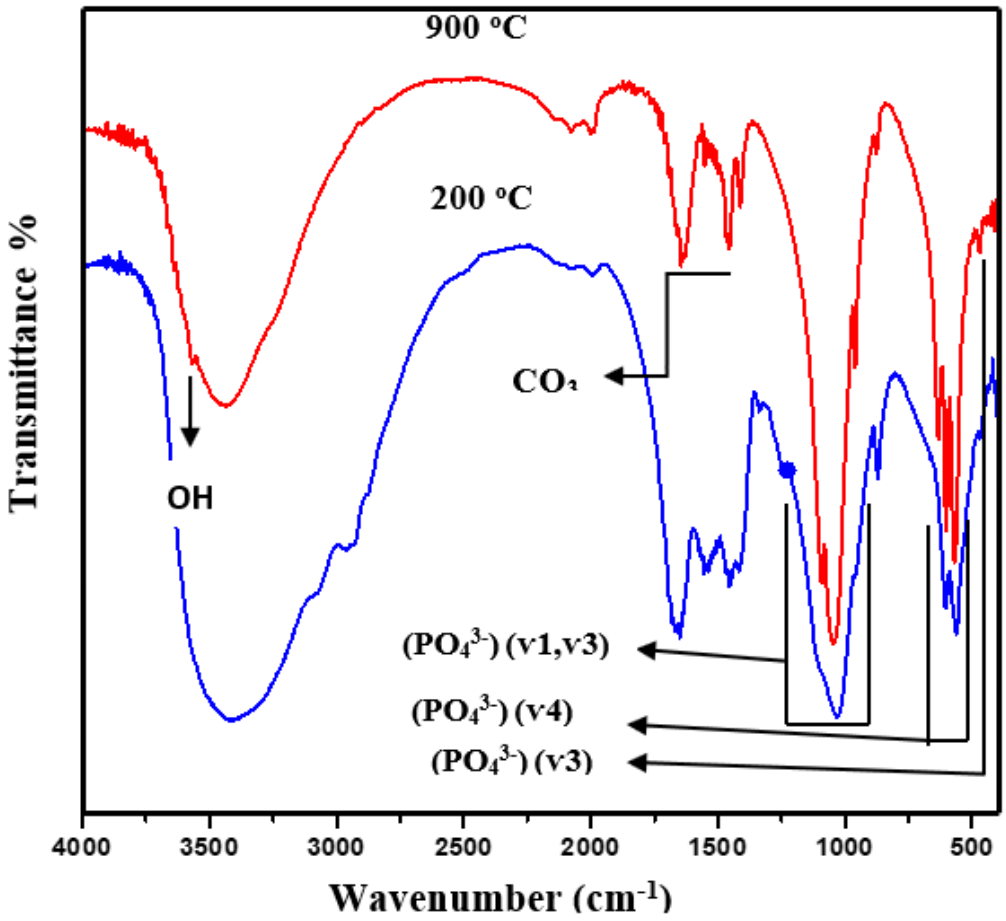


**Figure 3.2**: FTIR spectra of HA powder Calcined of BB 900°C for 2 h.

### 3.1.3 FESEM Analysis

FESEM micrographs of calcined extracted granules at 900°C revealed the particles to be densely packed, irregularly shaped agglomerates (Figure 3.3). The formation of HA particles may involve one or more of the subsequent processes: a) the synthesis of HA through the nucleation and growth processes as a result of (b) the Accumulation of constituent crystals via the molecular attractions of unique

scale forces, the surface free energy is diminished. As a result, the surface-free energy decreases. Aggregation occurs when additional crystals are generated within the aggregates as a result of continuous residual supersaturation. Subsequently, this agglomerated particle undergoes a process of coalescence with other particles, resulting in the formation of secondary particles that grow in size. The HA demonstrated a greater particle size and a spherical morphology. Grain growth and crystallization of HA particles were affected by an increase in calcination temperature as a result of thermal energy absorption during the chemical synthesis process. There are fewer visible fissures in the sample.

As time progresses, the volume of HA decreases significantly, while their surface-to-volume ratios increase substantially. Nevertheless, the presence of Van der Waals interactions coupled with these enormous surface areas produced a strong inclination towards agglomeration. Particle characteristics, including size, shape, and surface texture, are influenced by these factors. The particle size significantly influences the profile of drug release exhibited by the particles. Additionally, the morphology of HA particles is influenced by the bone source, calcination temperature, and holding duration.

An increase in calcination temperature results in the particulates achieving a finer consistency. Additionally, the dietary habits, gender, and age of the animals from which the bone was extracted could potentially exert an impact. Therefore, further research is necessary in order to comprehend the impact that these biological factors have on the morphology. Nonetheless, 900°C has been determined to be the optimal calcination temperature for isolating HA of the highest quality from BB.

### 3.1.4 Calcium-to-phosphorus ratio (Ca/P)

The elemental analysis performed using EDX permits the calculation of the Ca/P ratio, as shown in Table 3.3. The Ca/P ratio measured at 900 °C was 1.68, which can be attributed to the existence of these trace elements. The value that approaches the theoretical HA ratio of 1.67. During the calcination phase at 900°C, the monophase of HA began to persist, which led to a close Ca/P ratio.

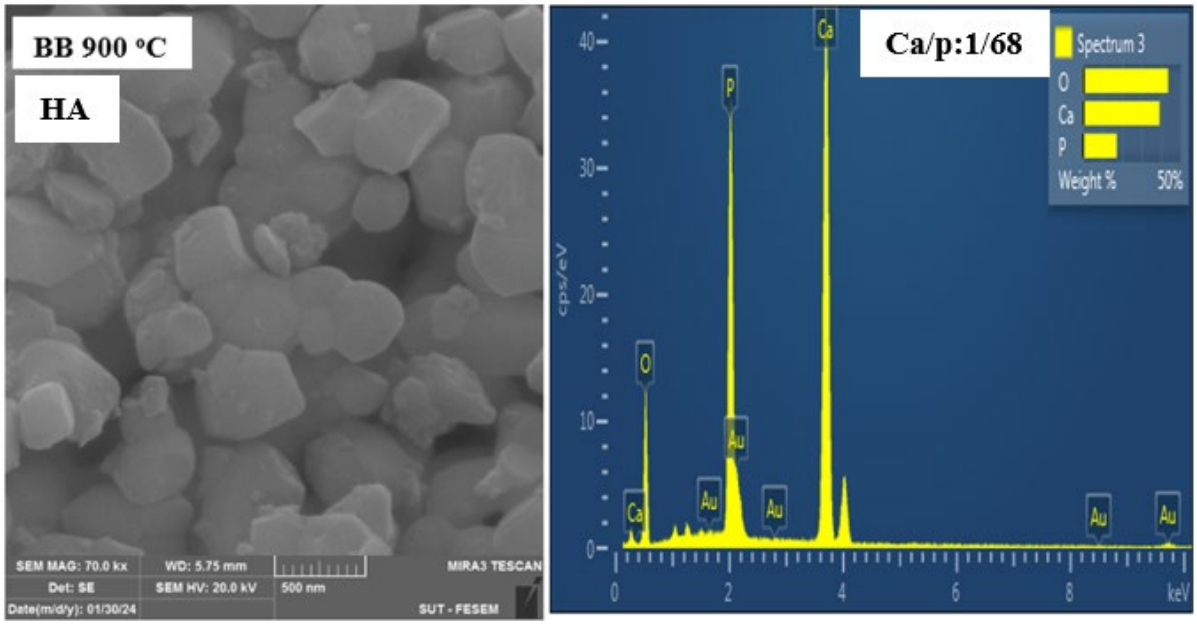


**Figure 3.3:** FESEM and EDX images showing the morphology and Ca/p of HA in BB 900˚C

**Table 3.3:** Ca/p ratio of calcined BB at 900 °C

| Samples BB | Elemental Composition (HA) (wt %) | | Ca/P ratio |
|---|---|---|---|
| | Ca | P | |
| 900 °C | 61.12 | 36.25 | 1.68 |

## 3.2 Dicalcium Phosphate Dihydrate (DCPD) Extracted from different sources

The findings and subsequent analysis of the dicalcium phosphate (DCPD) cements (brushite) derived from three distinct bone varieties are presented in this section. Table 3.4. Composition analysis, functional group analysis, and phase analysis are performed on the prepared cements. In contrast, parameters such as setting time, injectability, compressive strength, and in vitro characteristics of the prepared bone cement samples are detailed. A discussion of the in vitro bioactivity of the chosen DCPD cement in SBF for seven days is provided.

**Table 3.4** Description of DCP cement samples extracted from different sources

| Sample | Description |
|---|---|
| BB | DCPD extracted from bovine bone |
| LN | DCPD extracted from fish (Lethrinus Nebulosus, Forsskal 1775) (spangled emperor, FAO) |
| DP | DCPD extracted from fish (Diagramma pictum (Thunberg, 1792) |

## 3.3 Synthesis of Dicalcium Phosphate cement (DCPD) from bovine bone

### 3.3.1 Crystal Structure

XRD analysis of brushite phase as shown figure 3.4. brushite gives peaks at 22.13°, 29.66°, 30.80°, 34.54°, 37.25°, 41.78° and 42.35°, which were attributed to the (12 -1), (14 -1), (12 1), (150), (14 1), (15 -1) and (260) planes of crystalline brushite (JCDPS 72-0713) (figure 3.4). A small peak at 27.57° was assigned to the (2 0 0) plane to the monetite present as a minor secondary phase. The lattice data obtained for pure brushite confirmed the formation of monoclinic crystalline brushite with lattice parameters a= 5.099Å, *b*= 15.362 and *c*= 5.491 Å, $\alpha = \beta = 90^{\circ}$, and $\gamma = 120^{\circ}$ [5].

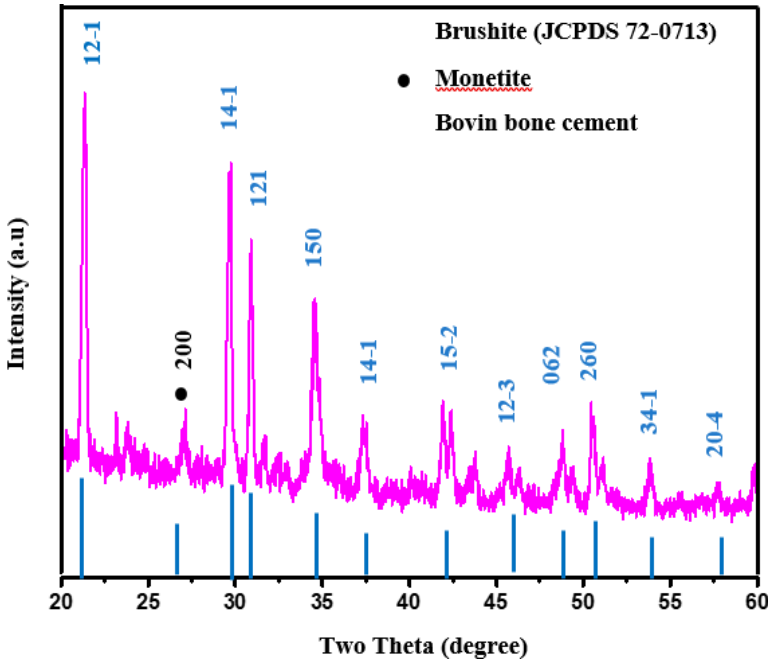


**Figure 3.4:** XRD patterns of brushite cements with reference pattern JCDPS 72-0713

## 3.3.2 FTIR spectra analysis

FTIR spectrum of brushite shown in Figure 3.5, Table 3.5 contained bands centred at 3547 and 3485cm$^{-1}$, which attributed the stretching of absorption water. Furthermore, the twist peak of water at 1648 cm$^{-1}$. phosphate peaks of brushite were establish at 1208, 1132, 1064, 981, 870, 658, 582 and 526 cm$^{-1}$.The bands at 1208–988 and 788–526 cm$^{-1}$ agree with, respectively, to v3 and v4 modes of vibration of phosphate groups. weakly peak at 981 and 870 cm$^{-1}$ were allocated to the P-OH extend of $HPO_4^-$ [6].

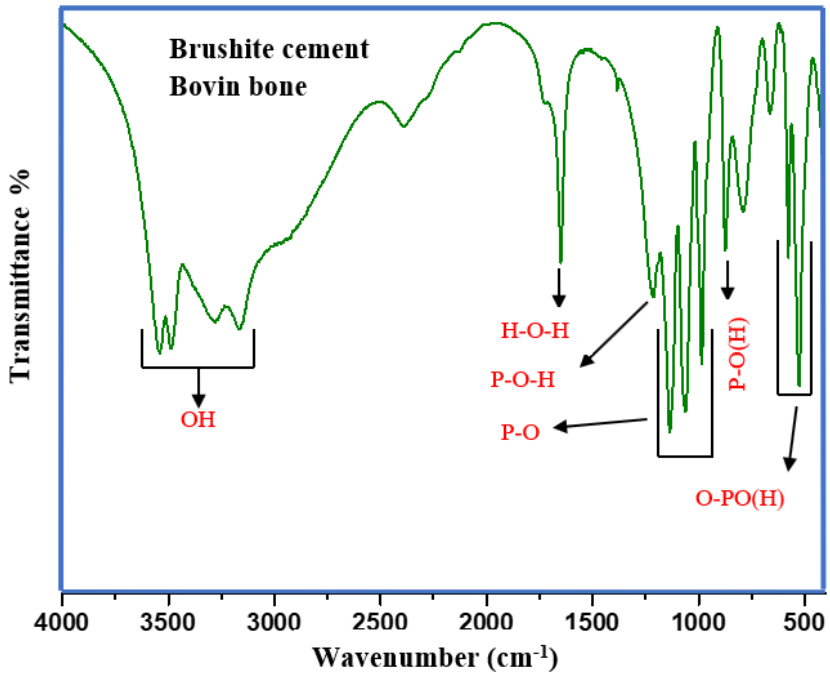


**Figure 3.5:** FT-IR spectra of brushite cement

**Table 3.5:** bands spectra of brushite

| Absorptions | FTIR bands |
|---|---|
| 3549-3475<br>3277-3155 | O-H stretching of lattice water molecules |
| 1620-1720(broad) | |
| 1653 | H-O-H bending of lattice |
| 1207 | water molecules<br>P-O-H in-plane bending |
| 1135 | P-O stretching |
| 1065 | |
| 984 | P-O stretching |
| 871 | P-O(OH) stretching |
| 784 | P-O(OH) out-of-plane |
| 663 | bending |
| 569 | Water liberations<br>O-P-O(H) bending mode |

### 3.3.3 Morphology

Due to the fact that brushite's chemical reactivity is highly dependent on its surface properties, regulating its crystal morphology is crucial for its use as a precursor to other bioceramics or as a functional material. The formation mechanism of nested structures is predicated not only on a reduction in concentration during crystallization, but also on the early aggregation of crystal nuclei. Controlling the early crystallization process, specifically the rate of nucleation, is thus the most significant determinant in determining the morphology

of the brushite crystals. Pure brushite FESEM images revealed the formation of small, irregularly shaped (Figure 3.6).

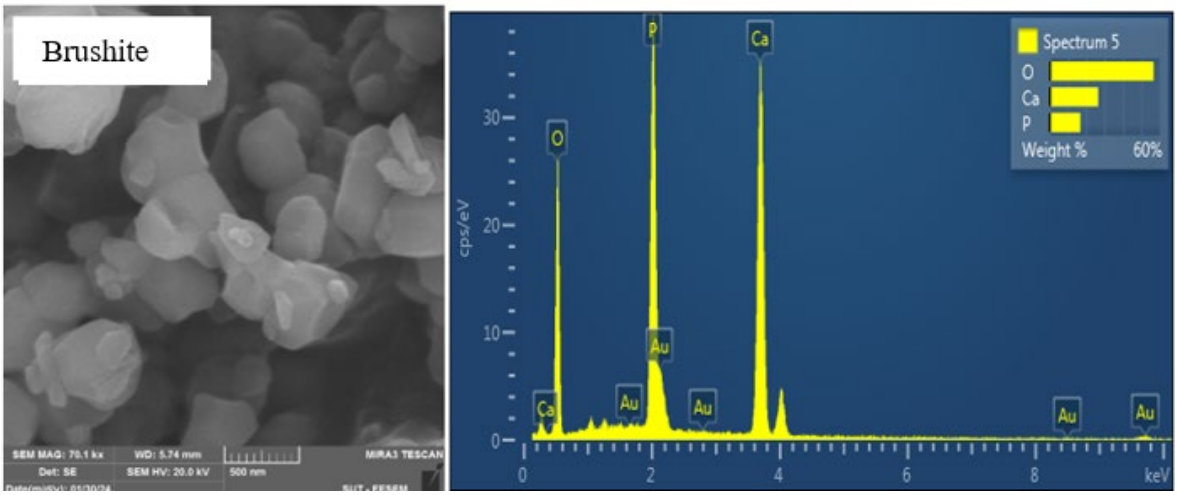


**Figure 3.6.** FESEM images and EDX of brushite cement

## 3.4 Mechanical properties

### 3. 4.1 Setting time and injectability

The clinical utility of brushite cements stems from their favorable solubility under physiological conditions. An objective of this study was to ascertain whether the setting reaction has any effect on the injectability of DCPD. Figure 3.7 illustrates the initial and ultimate configuration periods for DCPD at ambient temperature (25 $^{o}$C). At present, their expansive clinical application is constrained by several factors: prolonged setting periods, inadequate mechanical strength, and insufficient fluidity to facilitate administration via hypodermic needles. The results

of the cements' curing periods, as determined by the Gilmore needle, are illustrated in Figure 3.7. The pure brushite cement (sample 1) liquid-to-powder ratio exhibited initial and final curing durations of 2.03 minutes and 5.3 minutes, respectively. Brushite cement's rapid curing periods render it inappropriate for use in clinical settings. Conversely, incorporating varying concentrations of trisodium citrate into the brushite cement led to a significant delay in the setting process, as evidenced by the sample 3 final setting time of 12.3 minutes. Overall, it was observed that the ultimate configuration durations for samples 3, 4, and 5 were 20, 24, and 18 minutes, respectively. The findings suggest that the setting reaction can be influenced by the concentration of trisodium citrate $Na_3C_6H_5O_7$ in DCPD, leading to the formation of cement with distinct compositions.

The prolonged incorporation of injectable brushite cements into bone remodeling and their enhanced biodegradability make them highly promising as bone replacement materials. While brushite cement can be utilized in minimally invasive procedures, its mechanical strength and injectability are both inadequate. Controlling the injectability of cements and preventing the "filter-pressing" of particulate solid and liquid at syringe, which severely restricts their input via injection, It is recommended that the injection of material occur promptly following the blending of the liquid and granular components of the cement. Figure 3.7 illustrates that the injectability of the material rose from 12.22% to 35% (samples 1, 2), and then to 66%, 84%, and 78% (samples 3,4,5), respectively.
SBF.

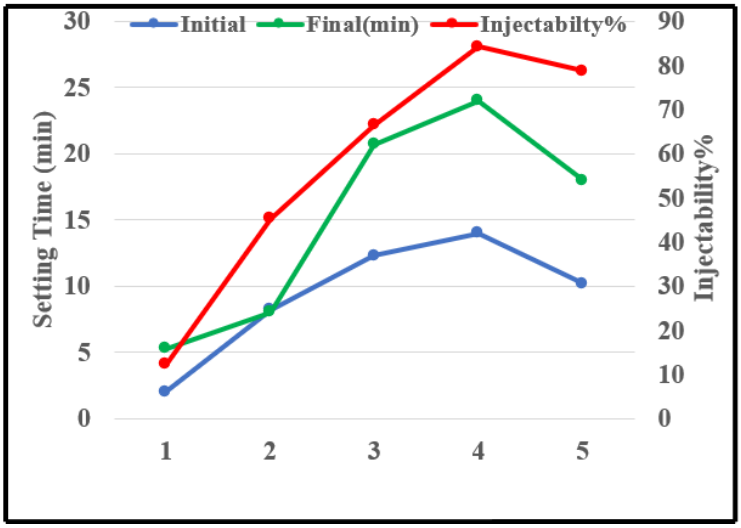


**Figure 3.7.** Setting time and injectability of brushite cements

### 3.4.2 Compressive strength

Table 3.6 and Figure 3.8 present the compressive strength of brushite cement prior to and subsequent to immersion in SBF for durations of 0, 1, 3, and 7 days. Sample 1 exhibited a compressive strength of 1.23 MPa of brushite prior to immersion in SBF solution. Sample 5's Brc sample, which had a compressive strength of 20.18 MPa, increased to 27.34 MPa after 7 days at immersion in SBF. Overall, brushite compressive strength increased to 33.75 MPa after three days of marinating in SBF.

**Table 3.6**: Compressive strength of brushite (MPa)

| Samples | 0 d | 1d | 3d | 7d | AVERAGE | STDEV |
|---|---|---|---|---|---|---|
| 1 | 1.23 | 8.4 | 13.52 | 17.24 | 10.0975 | 6.934043 |
| 2 | 10.35 | 15.7 | 20.37 | 18.82 | 16.31 | 4.422571 |
| 3 | 13.24 | 18.63 | 22.52 | 19.47 | 18.465 | 3.863543 |
| 4 | 18.27 | 24.21 | 31.45 | 18.32 | 23.0625 | 6.248367 |
| 5 | 20.18 | 26.22 | 33.75 | 27.34 | 26.8725 | 5.559792 |

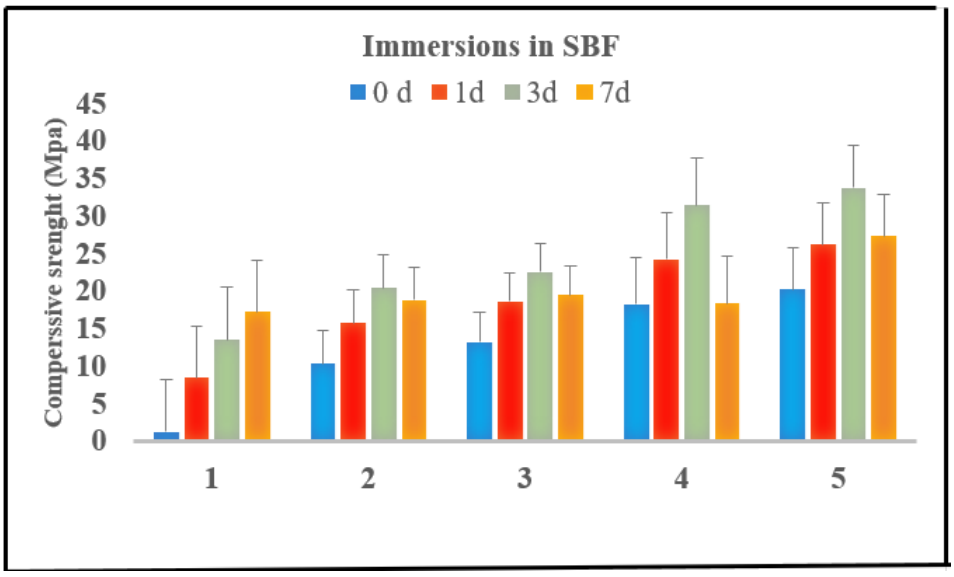


**Figure 3.8**: Compressive strength of brushite before and after immersion in SBF

### 3.4.3 Release of Ion from brushite cements

$Ca^{2+}$ release shown in table 3.7. The results showed that the dissolution of samples initiated immediately after 1 day of immersion of samples in the SBF solution. Increase in the amount of $Ca^{2+}$ ion release in the SBF solution was observed in 3day. However, gradual decrease in $Ca^{2+}$ was observed after 7days, which was attributed to formation of apatite layer.

**Table 3.7:** $Ca^{2+}$ ions release after 7 days at

| Time (day) | $Ca^{2+}$ ion (mg/L) in SBF |
|---|---|
| | Brc (BB) |
| 0.0 | 12.22 |
| 1 | 18.22 |
| 3 | 23.35 |
| 7 | 11.43 |

SD± 0.32-0.75

## *3.5 In vitro* controlled drug release

### *3.5.1* Antibiotic*s* release profiles from DCPD (BB 900)

An illustration of the cumulative release of cephalexin from DCPD is presented in Figure 3.9. The bimodal release profile was observed in this study, with a surge release occurring within the initial 12 hours, succeeded by a controlled continuous release thereafter. Following an initial 12-hour rapid release of 70% cephalexin, the rate of release subsequently slowed, culminating in a cumulative release of 81% after a duration of 7 days. The rapid, release of the drug was ascribed to antibiotic release occurring at DCPD matrix, whereas the start explosive release was ascribed to drug release occurring on the exterior surface of the samples. It is believed that a burst release during the initial phase, followed by a gradual release over the course of seven days, is optimal for preventing bacterial infection following surgery. There are three potential explanations proposed for the sluggish release of the substance from DCPD: (i) the formation of an antibiotic-calcium phosphate complex through the interaction of organic acid molecules and calcium ions; (ii) the antibiotic's low water solubility;

and (iii) the transformation of the loaded matrix into apatite phase, which occurs when the DCPD reactants undergo a change in composition. Antibiotic molecules could potentially become ensnared in the apatite crystals [117D].

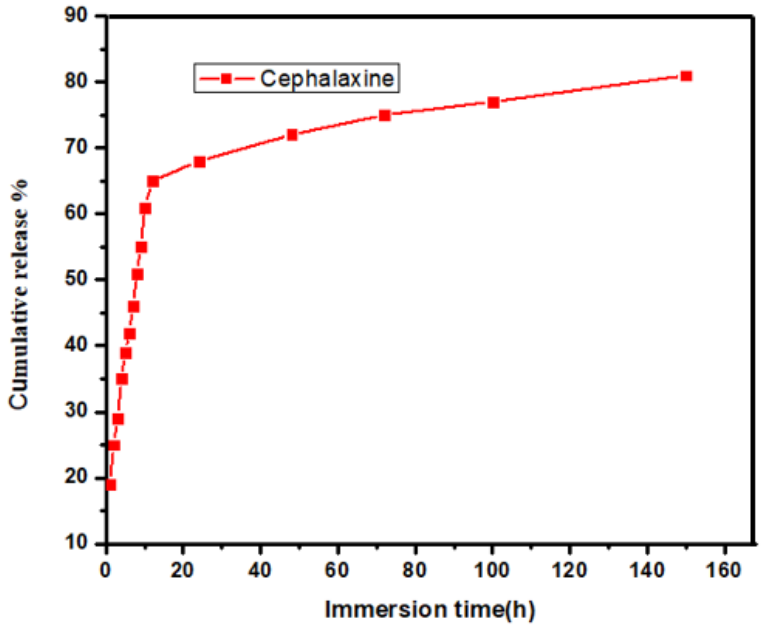


**Figure 3.9** *In vitro* release profile of antibiotics from DCPD calcined (BB 900˚C)

## 3.6 Extraction of Hydroxyapatite (HA) from fish (Lethrinus Nebulosus (LN)

HA was extracted from fish (LN) (Lethrinus Nebulosus Forsskal 1775) (spangled emperor, FAO) inhabiting the Arabian Gulf (Barash) in southern Iraq via the calcination procedure. The bone powder underwent the calcination process, during which the unprocessed powder was subjected to furnace heating at varying temperatures of 200, 700, and 900 °C for a duration of 5 hours at a rate of 5 °C/min.

HA was extracted from fish using the calcination method for a duration of 2 hours at temperatures of 200 °C and 900 °C.

### 3.6.1 X-Ray Diffraction (XRD) Analysis

A phase analysis of the HA was performed utilizing XRD technology (Figure 3.10). Successful crystallization of HA is achieved through calcination at temperatures ranging from 900 ºC. The XRD pattern of crystalline HA revealed distinct peaks at the following coordinates: (26.12 º), (28.45 º), (31.15 º), (33.20 º), (34.28 º), (40.11 º), (46 v), (49.47 º), and (55 º). These peaks were identified as representing the (002), (210), (211), (300), (202), (310) and (222), (213), and (304) planes, respectively. The lattice parameters and diffraction peaks exhibited a high degree of concordance with the standard phase of HA (JCDPS 09-432). In conjunction with the primary peaks of HA, a minuscule peak at 30.71º was detected as the calcination degree increased to 900ºC. This peak may have been caused by the (0210) diffraction plane of β-tricalcium phosphate (β-TCP), as identified by (JCDPS No. 09-0169). The β-TCP phase is generated as a minor byproduct through the decomposition of HA at elevated temperatures [113]. Moreover, with respect to crystallite size, degree of crystallinity, and lattice parameters, no substantial alterations were noted (Table 3.8).

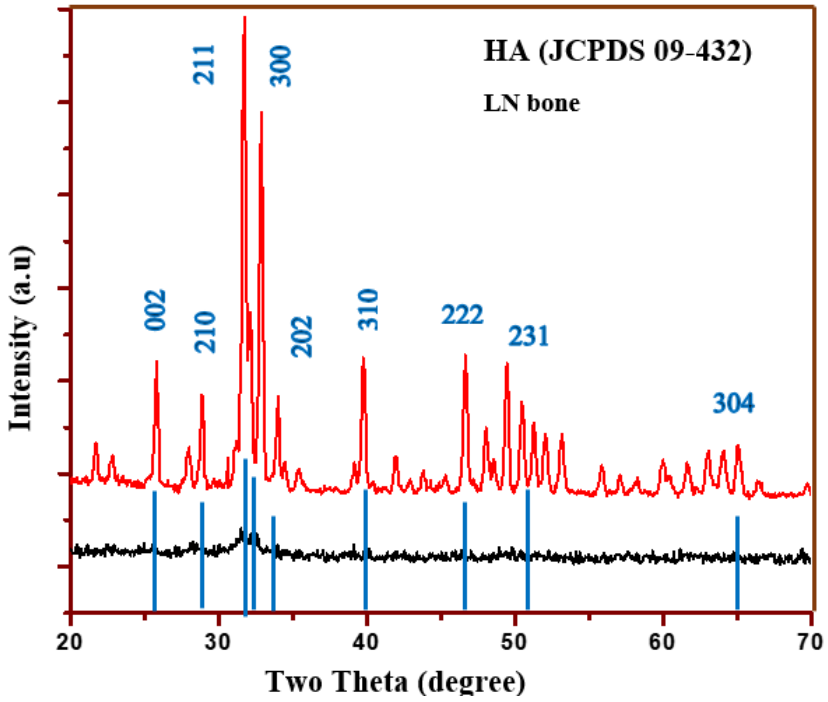


**Figure 3.10**: XRD pattern of (HA)from fish bones (LN) calcined at 900 ˚C for 2 h.

**Table 3.8:** Lattice parameters, dgree of crystallinity and crystallite size.

| Sample ID | Lattice parameters | | | $X_c$ (%) | *CS* (nm) |
|---|---|---|---|---|---|
| | *a* (Å) | *c* (Å) | *V* (Å)$^3$ | | |
| Standard HA | 9.418 | 6.884 | 528.8 | - | - |
| HA-900 | 9.416 | 6.863 | 527.3 | 88.77 | 30.04 |

- $X_c$ = degree of crystallinity; *CS* = crystallite size.

## 3.6.2 FTIR spectra analysis

FTIR analysis was employed to identify the functional groups present in the extracted HA; the corresponding outcomes are illustrated in Figure 3.11. At 468 cm$^{-1}$ for the phosphate ($PO_4^{3-}$) group ($PO_4^{3-}$ (v4)), 567 cm$^{-1}$ for the phosphate ($PO_4^{3-}$) group

(ν2), 608 $cm^{-1}$ for the phosphate ($PO_4^{3-}$) group (ν2), and 921-1200 $cm^{-1}$ for the phosphate ($PO_4^{3-}$) group (ν1,3), four vibrational modes were detected. 3569 $cm^{-1}$ and 637 $cm^{-1}$, the bending and stretching of the hydroxyl (OH) group were identified, respectively. Additionally, carbonate ($CO_3^{2-}$) vibrational modes were identified at 1408 $cm^{-1}$ and 1520 $cm^{-1}$. However, it is conceivable that the existence of $CO_3^{2-}$ actually amplifies the biological of HA; therefore. Phosphate and hydroxyl band sharpness indicated the formation of crystalline HA. The $PO_4^{3-}$group exhibited enhanced sharpness at 900 °C calcination temperatures, a result that may be ascribed to an increased degree of crystallinity (Table 1).

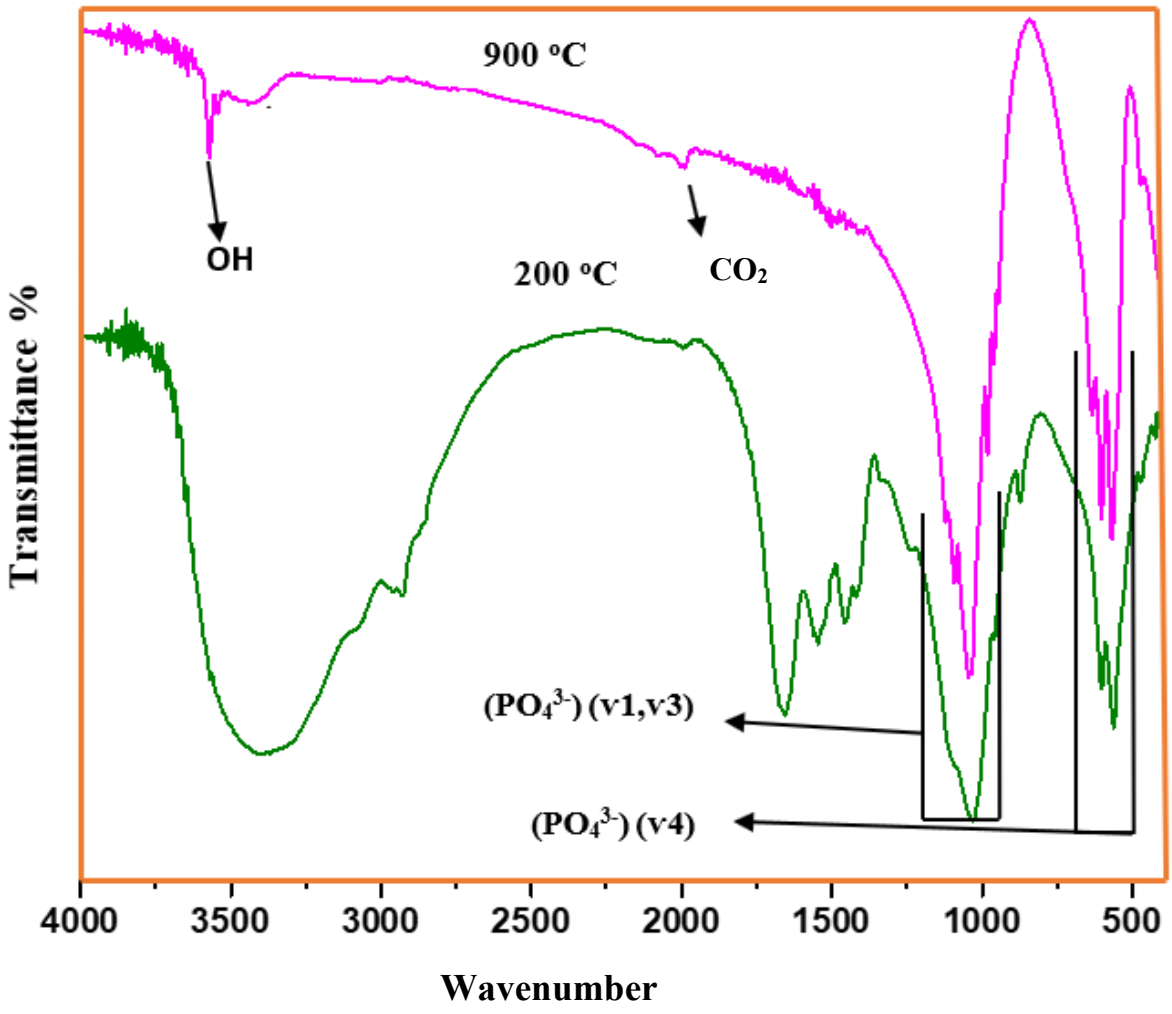


**Figure 3.11:** FTIR spectra of HA at 900 °C

### 3.6.3 Morphological Analysis

Micrographs FESEM revealed the particles to be densely packed, shaped conglomerate (Figure 3.12). The formation of HA particles may involve one or more of the subsequent processes: a) the synthesis of HA through the nucleation and growth processes. As a result of (b) the accumulation via the molecular

attractions, the surface free energy is diminished. As a result, the surface-free energy decreases [114]. Aggregation occurs when additional crystals are generated within the aggregates as a result of continuous residual supersaturation. This agglomerated particle subsequently forms secondary particles through collisions with other particles., which subsequently increase in size.

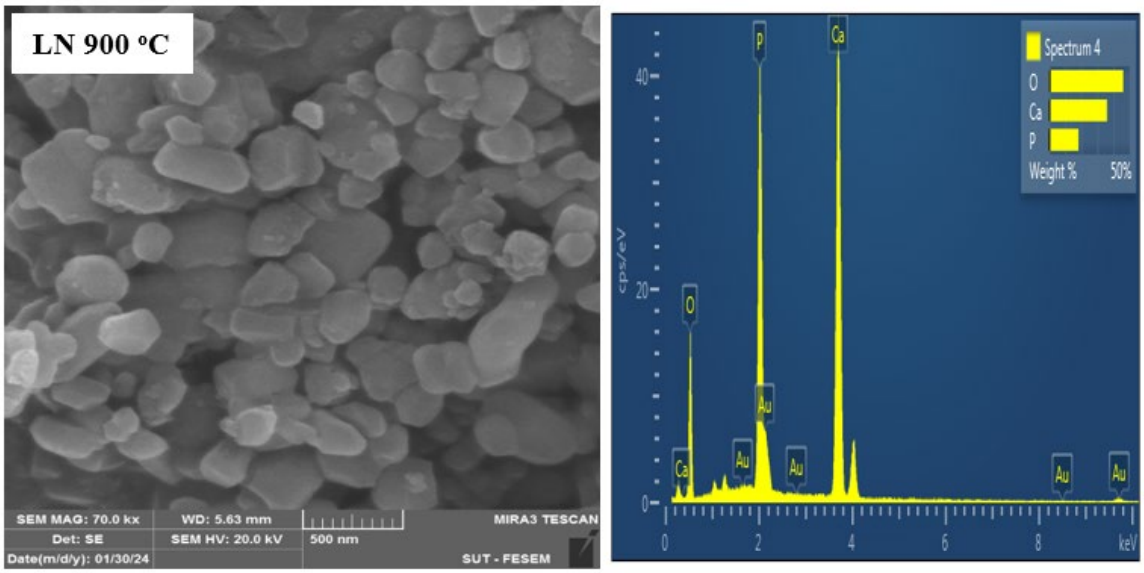


**Figure 3.12:** FESEM images and EDX of HA-900°C.

## 3.6.4 Calcium-to-phosphorus ratio (Ca/P)

The hydroxyapatite (HA) Ca/P atomic ratio was ascertained through the utilization of energy disperse X-ray (EDX). The elements that were found to be most prevalent in the fish bone are calcium and phosphorus, as illustrated in Figure 3.12. The chemical formula of hydroxyapatite, which serves as a standard, indicates that the molar ratio of calcium to phosphorous is approximately 1.67 [76]. The outcomes of the EDX analysis conducted on the acquired apatite are illustrated in

Figure 3.12. The figure illustrates that the apatite produced via the calcination method had a Ca/P ratio of 1.68 at 900 °C. These values are considered to be within the acceptable range for hydroxyapatite. The deviation of these values from the standard HA value could potentially be attributed to the carbonate group being incorporated into the apatites produced using those techniques [79]. Nevertheless, recent findings validate the notion that the apatite produced via calcination is virtually devoid of carbonate. Consequently, the Ca/P molar ratio of the apatite obtained via this method is in close proximity to the standard value listed in Table 3.9.

**Table 3.9:** Ca/p ratio of (HA) calcined (LN) at 900 °C

| Samples FB | Elemental Composition (wt %) | | Ca/P ratio |
|---|---|---|---|
| | Ca | P | |
| 900 °C | 61.12 | 36.25 | 1.68 |

## 3.7 Synthesis of Dicalcium Phosphate cement (DCP) from (LN) bone

### 3.7.1 X-Ray Diffraction (XRD) Analysis

By using XRD brushite Phase analysis as shown in figure 3.13. The peaks at 21.18°, 29.64°, 30.85°, 34.40°, 37.23°, 41.75° and 42.35°, were attributed to the (1 2-1), (14-1), (121), (150), (141), (15-1) and (260) degree of crystallinity (JCPDS

72-0713) (figure 3.13). Brushite observed the lattice data confirmed of monoclinic crystalline brushite with lattice parameters a= 5.099Å, *b*= 15.362 and *c*= 5.491 Å, α = β = 90° , and γ =120°.

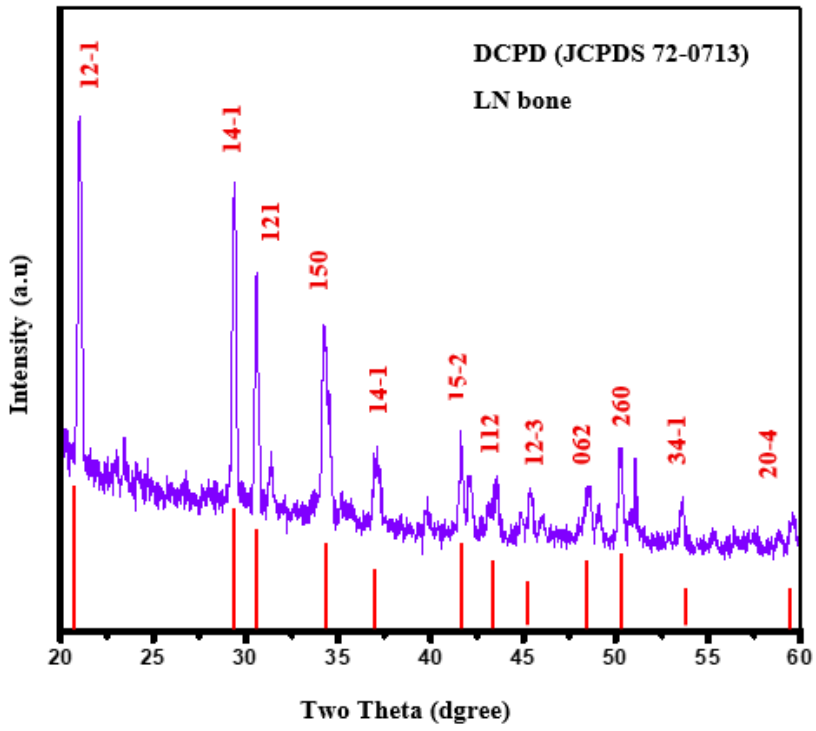


**Figure 3.13:** XRD patterns of brushite cements with reference pattern JCDPS 72-0713

## 3.7.2 FTIR spectra analysis

FTIR spectrum of brushite shown in Figure 3.14 contained bands centred at 3547 and 3485cm$^{-1}$, which allocate to the extent of water and. Furthermore, the band of $H_2O$ was located at 1646 cm$^{-1}$. bands phosphate of brushite were located at 1211, 1135, 1066, 985, 876, 660, 584 and 528 cm$^{-1}$.The bands at 1208–988 and

789–528 $cm^{-1}$ to $\nu_3$ and $\nu_4$ vacillation of groups phosphate. Weakly peak at 985 and 875 $cm^{-1}$ were allocated to the P-OH extend of $HPO_4^-$.

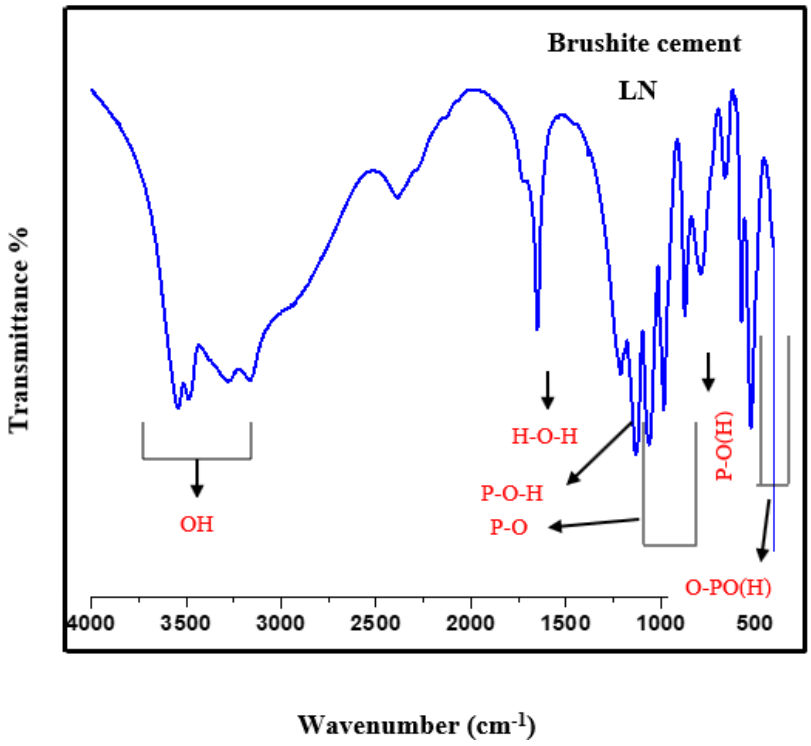


**Figure 3.14:** FT-IR spectra of brushite cement (LN)

### 3.7.3 Morphology

Due to the fact that brushite's chemical reactivity is highly dependent on its surface properties, regulating its crystal morphology is crucial for its use as a precursor to other bioceramics or as a functional material. The formation mechanism of nested structures is predicated not only on a reduction in concentration during crystallization, but also on the early aggregation of crystal nuclei. Controlling the early crystallization process, specifically the rate of

nucleation, is thus the most significant determinant in determining the morphology of the brushite crystals. Pure brushite FESEM images revealed the formation of small, irregularly shaped, structured particles. (Figure 3.15).

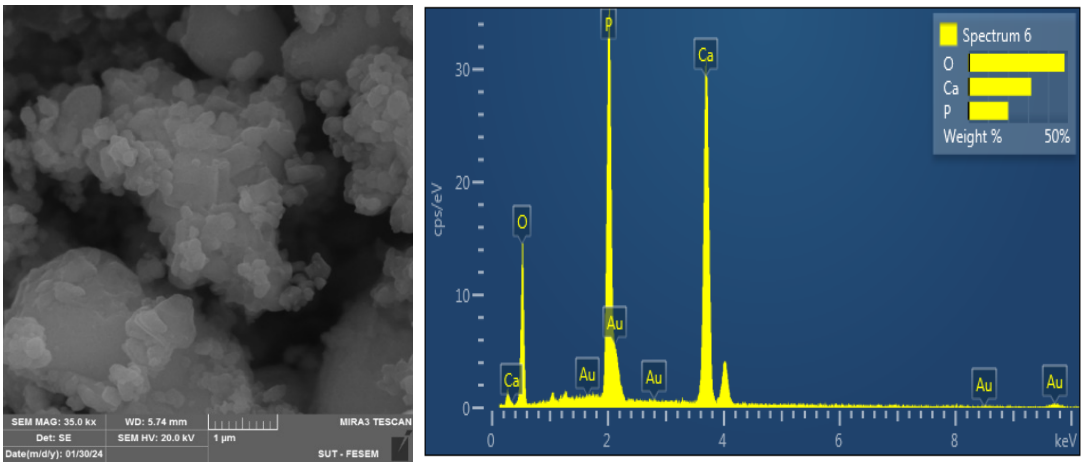


**Figure 3.15.** FESEM images and EDX of brushite cement

## *3.8 In vitro study*

### 3. 8.1 Setting time and injectability

The clinical utility of brushite cements stems from their favorable solubility under physiological conditions. An objective of this study was to ascertain whether the setting reaction has any effect on the injectability of DCPD. Figure 3.16 illustrates the initial and ultimate configuration periods for DCPD at ambient temperature (25 ◦C). At present, their expansive clinical application is constrained by several factors: prolonged setting periods, inadequate mechanical strength, and insufficient fluidity to facilitate administration via hypodermic needles. The results of the cements' curing periods, as determined by the Gilmore

needle, are illustrated in Figure 3.16. The pure brushite cement (sample 1) liquid-to-powder ratio exhibited initial and final curing durations of 2.3 minutes and 4 minutes, respectively. Brushite cement's rapid curing periods render it inappropriate for use in clinical settings. Conversely, incorporating varying concentrations of trisodium citrate into the brushite cement led to a significant delay in the setting process, as evidenced by the sample 2 final setting time of 6.7 minutes. Overall, it was observed that the ultimate configuration durations for samples 3, 4, and 5 were 20, 24, and 18 minutes, respectively. The findings suggest that the setting reaction can be influenced by the concentration of trisodium citrate in DCPD, leading to the cement formation with distinct composite.

The prolonged incorporation of injectable brushite cements into bone remodeling and their enhanced biodegradability make them highly promising as bone replacement materials. While brushite cement can be utilized in minimally invasive procedures, its mechanical strength and injectability are both inadequate. Controlling the injectability of cements and preventing the "filter-pressing" of particulate solid and liquid within the syringe. It is recommended that the injection of material occur promptly following the blending of the liquid and granular components of the cement. As shown in Figure 3.16, the injectability of the material rose from 12.22% to 35% (samples 1, 2), and then to 66%, 84%, and 78% (samples 3,4,5), respectively.

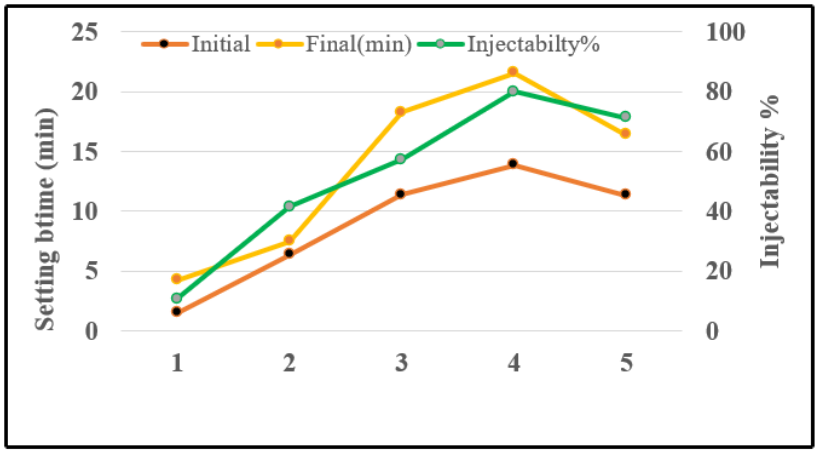


**Figure 3.16.** Setting time and injectability of brushite cements

### 3.8.2 Compressive strength

Table 3.10 and Figure 3.17 present the compressive strength of brushite cement prior to and subsequent to immersion in SBF for durations of 0, 1, 3, and 7 days. Sample 1 exhibited a compressive strength of 16.54 MPa of brushite prior to immersion in SBF solution. Sample 5's brushite exhibits an increase in compressive strength from 20.18 to 22.45 MPa after 7 days of immersion in SBF. Overall, Brc compressive strength increased to 33.75 after three days of marinating in SBF.

**Table 3.10**: Compressive strength of brushite duration 7 days

| ID Samples | 0 d | 1d | 3d | 7d | AVERAGE | STDEV |
|---|---|---|---|---|---|---|
| 1 | 0.98 | 6.4 | 11.25 | 16.54 | 8.79 | 5.76 |
| 2 | 8.32 | 10.15 | 17.65 | 15.79 | 12.97 | 3.85 |
| 3 | 11.54 | 14.76 | 20.11 | 19.12 | 16.38 | 3.44 |
| 4 | 15.22 | 19.81 | 33.75 | 18.32 | 19.35 | 3.17 |
| 5 | 17.56 | 20.18 | 27.43 | 22.45 | 22.40 | 3.49 |

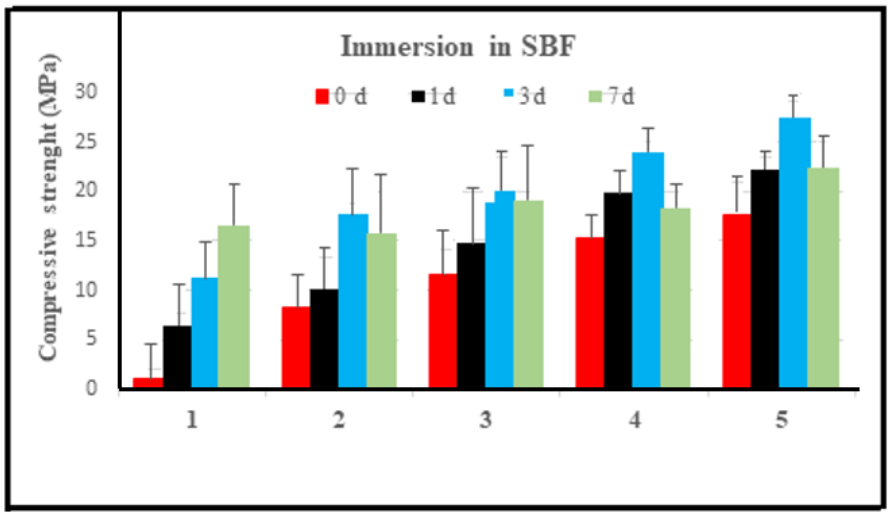


**Figure 3.17**: Compressive strength of brushite before and after immersion in SBF

## 3.8.3 $Ca^{2+}$ ion release from cements

Table 3.11 details the calcium release in SBF over a period of seven days. The findings indicated that the solubility of the samples commenced promptly one day following their immersion in the SBF solution. A three-day increase in the quantity of $Ca^{2+}$ ion discharge was detected in the SBF solution. After seven days, however,

a progressive decline in $Ca^{2+}$ was observed, which was likely attributed to their utilization during the formation of the apatite stratum.

**Table 3.11:** $Ca^{2+}$ ions release

| Immersion time (day) | Release of $Ca^{2+}$ ion (mg/L) in SBF |
|---|---|
| | Brc (BB) |
| 0.0 | 12.22 |
| 1 | 18.22 |
| 3 | 23.35 |
| 7 | 11.43 |

SD± 0.32-0.75

## 3.9 *In vitro* controlled drug release

### 3.9.1 *In vitro* antibiotics release profiles of DCPD (LN 900°C)

The figure depicting the cumulative release of cephalexin from DCPD is Figure 3.18. The bimodal release profile was observed in this study, with a surge release occurring within the initial 12 hours, succeeded by a controlled continuous release thereafter. Following an initial 12-hour rapid release of 80% cephalexin, the rate of release subsequently declined, culminating in a cumulative release of 96.3% after a duration of 7 days. The gradual, speed release of the antibiotic was attributed to antibiotic release occurring the cement network, as opposed to the initial explosive release which was ascribed to drug release occurring on the exterior surface of the samples. It is believed that a burst release during the initial phase, followed by a gradual release over the course of seven days, is optimal for preventing bacterial infection following surgery. There are three potential factors that could account for

the antibiotic's sluggish release from cement: (i) the formation of an antibiotic-calcium phosphate complex through the interaction of organic acid molecules with calcium ions; (ii) the antibiotic's weak solubility in water; and (iii) The alteration in the characteristics of the laden matrix, specifically the transformation of the cement reactants into the apatite phase. Antibiotic molecules could potentially become ensnared in the apatite crystals.

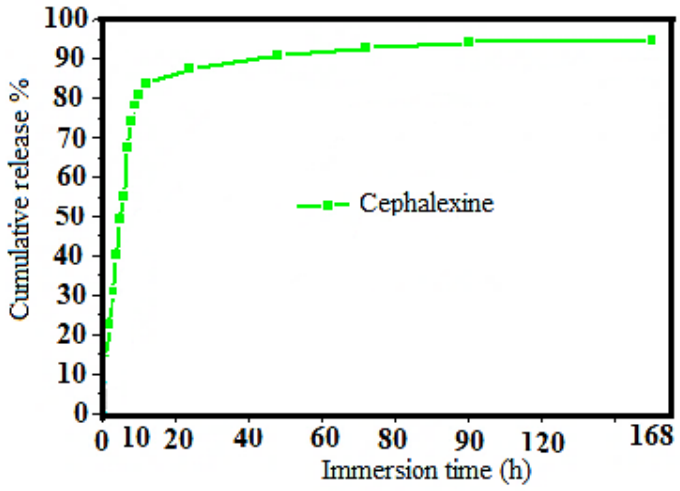


**Figure 3.18** *In vitro* release profile of antibiotics from DCPD calcined (LN 900°C)

## 3.10 Extraction of Hydroxyapatite (HA) from fish (DP) (Diagramma pictum (Thunberg, 1792) bone

### 3.10.1 X-Ray Diffraction (XRD) Analysis

Following dehydration, the bones of Diagramma pictum (Thunberg, 1792) (DP) underwent calcination in an electric furnace for two hours at temperatures of

900 °C. XRD was utilized of determine phase HA particles that had been calcined at 900 °C (Figure 3.19). Validation of the XRD patterns was accomplished through a comparison with the HA standard (ICDD 00-003-0747). All peaks observed at temperatures of 900 °C are consistent with the standard HA peaks; the Miller indices for the peaks with the greatest intensities are as follows: (002), (210), (211), (300), (202), (310), (222), (231), and (304). Thus, it is confirmed that the sample analyses by XRD at calcination temperatures of 900 °C consisted entirely of HA phases. The lattice parameters and diffraction peaks exhibited a high degree of concordance with pdf standard of HA (JCDPS 09-432). Calcination temperature increased, so did the intensity of the XRD peak, which indicated that the sample's crystallinity also increased. The principal peaks at 900 °C represent a form of HA. Nevertheless, at this temperature, beta tri-calcium phosphate (β-TCP) begins to manifest as modest peaks. This is due to the HA decomposition process, which commenced at a specific temperature and resulted in the production of β-TCP. Some studies indicate that HA decomposes into β-TCP when exposed to heat [119].

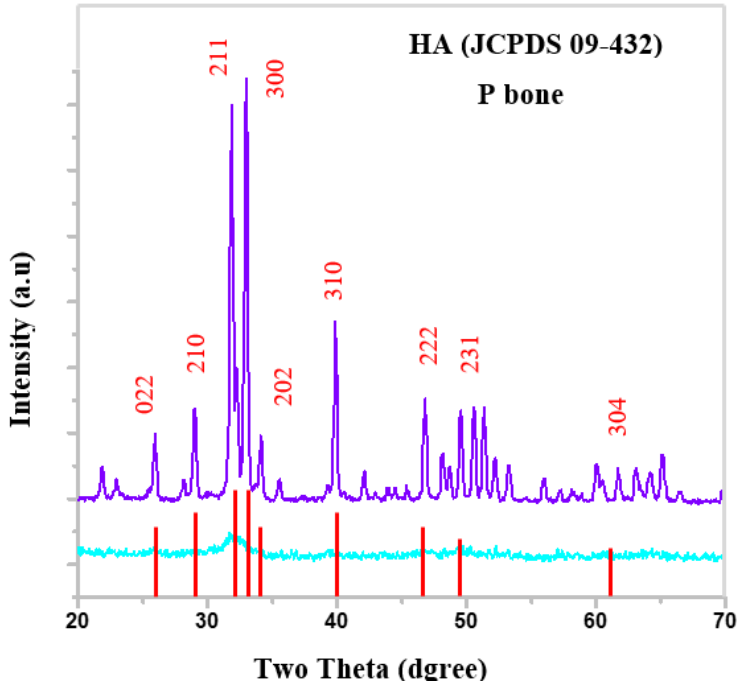


**Figure 3.19**: XRD pattern of P bones calcined at 900 ̊C for 2 h.

**Table 3.12:** Lattice parameters of HA from P bone (DP) calcined at 900 ̊C plus degree of crystallinity.

| Samples | Chemical formula | Lattice Parameter | | | $X_c$ | *D* |
|---|---|---|---|---|---|---|
| | $Ca_{10}(PO_4)_6(OH)_2$ | *a* (Å) | *c* (Å) | *V* (Å)$^3$ | (%) | (nm) |
| Standard HA | $Ca_5(PO_4)_3(OH)$ | 9.418 | 6.884 | 528.8 | ---- | ---- |
| HA (900) | $Ca_{10}(PO_4)_6(OH)_2$ | 9.419 | 6.875 | 527.7 | 86 | 97.22 |

## 3.10.2 FTIR analysis

The FTIR spectra of HA calcinated at two distinct temperatures (900°C) are illustrated in Figure 3.20. The spectra of unheated DP bone and heated fish bone are distinguishable, as illustrated in Figure 3.20, because heat treatment induces

modifications in the chemical bonds of the bones. Upon undergoing calcination, bone particles transform visually from a yellowish white hue to a pure white hue. The FTIR spectra additionally demonstrate the existence of hydroxyl ($OH^-$) and phosphate ($PO_4^{3-}$) groups. The clarity of these spectra is enhanced in calcinated samples due to the destruction of the cross-linked structure in the fish bone during the calcination process. A total of four vibrational modes associated with the phosphate ($PO_4^{3-}$) group were identified: 980-1200 $cm^{-1}$ ($PO_4^{3-}$ (ν1,3)), 520 $cm^{-1}$ ($PO_4^{3-}$ (v2)), 486 $cm^{-1}$ ($PO_4^{3-}$ (v2), and 534 $cm^{-1}$ ($PO_4^{3-}$ (ν4)) found in 3577 $cm^{-1}$ and 644 $cm^{-1}$, the bending and stretching the hydroxyl (OH) group were observed, respectively. The hydroxyl group is associated with the pointed, narrow band at 3572 $cm^{-1}$, which indicates the presence of the HA phase.

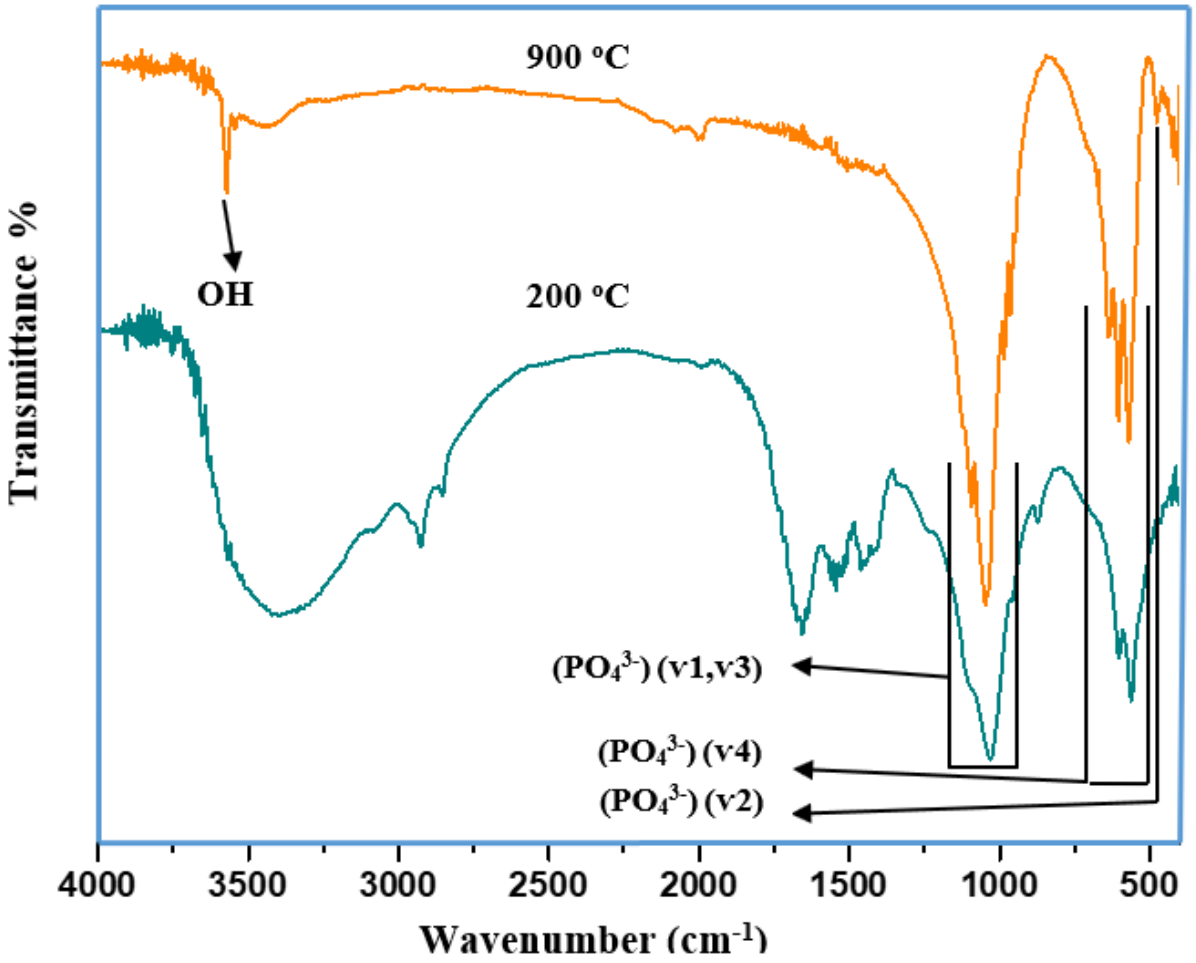


**Figure 3.20:** FTIR spectra of DP - 900 ˚C materials

### 3.10.3 FESEM Analysis

Using FESEM, the morphology of the HA extracted from DP bone was examined. As shown by the FESEM micrograph in Fig. 3.21, the HA material at all calcination temperatures (900 °C) has an irregular shape. At a temperature of 900 °C, an irregular HA with an asymmetrical shape is visible. Powder particle diameters varied between 300 and 530 nanometers. With increasing calcination temperature, the bulk of HA

also increases. As the temperature increased, the HA particles tended to aggregate, as shown in the FESEM micrograph in Figure 3.21. Furthermore, Venkatesan et al. proposed that the expansion of particles occurs when organic constituents are entirely eliminated via the calcination process [120]. This finding is consistent with the result depicted in Figure 3.21, which indicates that an increase in temperature leads to a corresponding increase in particle size.

The HA demonstrated a greater particle size and a spherical morphology. Grain growth and crystallization of HA particles were affected by an increase in calcination temperature as a result of thermal energy absorption during the chemical synthesis process. There are fewer visible fissures in the sample.

As time progresses, the volume of HA decreases significantly, while their surface-to-volume ratios increase substantially. Nevertheless, the presence of Van der Waals interactions coupled with these enormous surface areas produced a strong inclination towards agglomeration. Particle characteristics, including size, shape, and surface texture, are influenced by these factors. The particle size significantly influences the profile of drug release exhibited by the particles. Additionally, the morphology of HA particles is influenced by the bone source, calcination temperature, and holding duration. An increase in calcination temperature results in the particulates achieving a finer consistency. Additionally, the dietary habits, gender, and age of the animals from which the bone was extracted could potentially exert an impact. Therefore, further research is necessary in order to comprehend the impact that these biological factors have on the morphology. Nonetheless, 900°C has been determined to be the optimal calcination temperature for isolating HA of the highest quality.

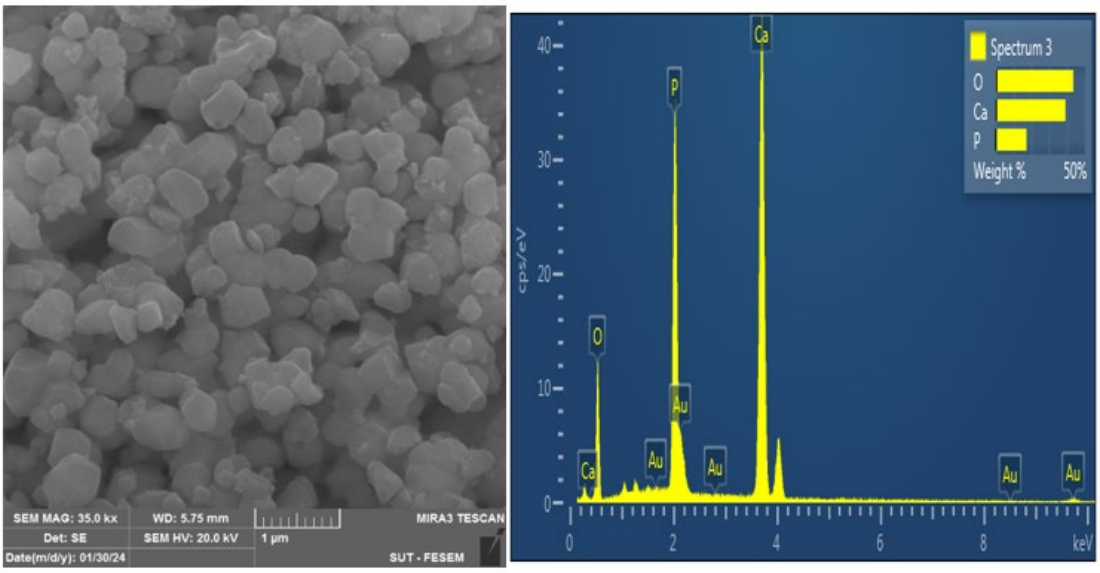


**Figure 3.21:** FESEM images and EDX of DP-900°C.

## 3.10.4 Calcium-to-phosphorus ratio (Ca/P)

The hydroxyapatite (HA) Ca/P ratio was ascertained through the utilization of energy disperse spectroscopy (EDX). The elements that were found to be most prevalent in the fish bone are calcium and phosphorus, as illustrated in Figure 3.21. The chemical formula of the standard hydroxyapatite indicates that the molar ratio of calcium to phosphorous is roughly 1.67 in theory. The outcomes of the EDX analysis conducted on the acquired apatite are illustrated in Figure 3.21. The Ca/P ratio for hydroxyapatite, as indicated in Table 3.13, was 1.66 for apatite produced via subcritical water and 1.63 for alkaline hydrothermal processes at temperatures of 900 $^{o}$C, respectively. These values fall within the acceptable range. The discrepancy between these values and the standard HA value could potentially be attributed to the carbonate group being incorporated into the apatites produced via those procedures. However, recent evidence confirming that the apatite produced through calcination is

nearly carbonate-free indicates that the Ca/P molar ratio of the apatite obtained via this method is extremely close to that of the standard. The successful elemental mapping of pure phases confirmed the HA structure, which was further validated by the sample's Figure 3.21, which illustrates the homogeneous distribution of Ca, P, and O elements.

**Table 3.13:** Ca/p ratio of calcined DP at 900 $^{o}$C

| Samples CB | Elemental Compostion (wt %) | | Ca/P ratio |
|---|---|---|---|
| | Ca | P | |
| 900 $^{O}$C | 62.33 | 37.38 | 1.66 |

## 3.11 Synthesis of Dicalcium Phosphate cement (DCPD) from (DP) bone

### 3.11.1 X-Ray Diffraction (XRD) Analysis

XRD Phase analysis of the cement as shown in figure 3.22. The XRD pattern of brushite contained peaks at 22.17°, 28.57°, 31.82°, 35.25°, 38.224°, 42.77° and 43.29°, which were ascribed to the (12 -1), (14 -1), (12 1), (15 0), (141), (15-1) and (2 6 0) planes of crystalline brushite (JCDPS 72-0713) (figure 3.22). The lattice data obtained for pure brushite confirmed the formation of monoclinic crystalline brushite with lattice parameters a= 5.099Å, *b*= 15.362 and *c*= 5.491 Å, $\alpha = \beta = 90^{\circ}$, and $\gamma = 120^{\circ}$.

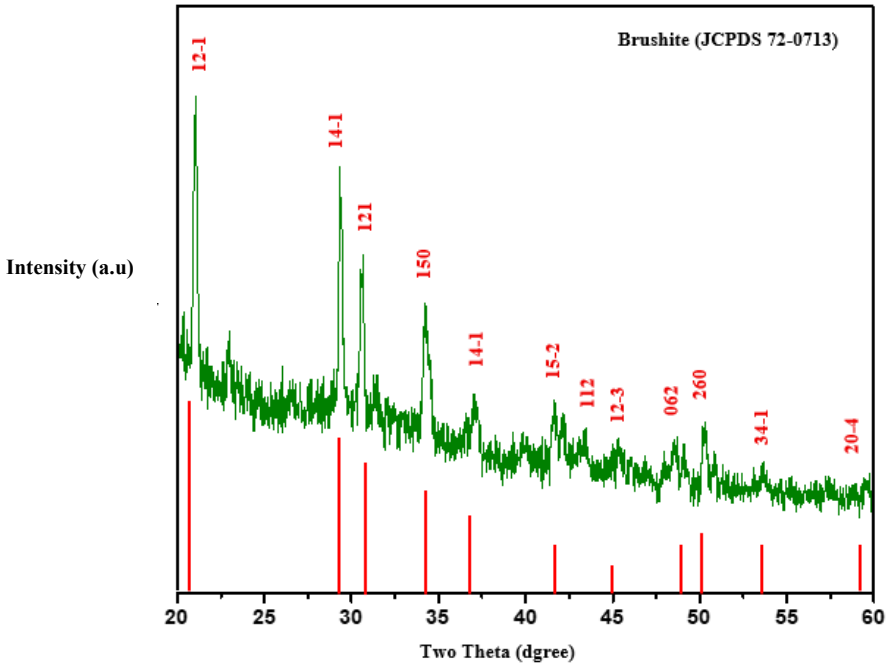


**Figure 3.22:** XRD patterns of brushite cements with reference pattern JCDPS 72-071

## 3.11.2 FTIR spectra analysis

FTIR spectrum of brushite shown in Figure 3.23 contained bands centred at 3547 and 3485cm$^{-1}$, which attributed to the extended to adsorption water, the twist peak of $H_2O$ was shown at 1659 cm$^{-1}$. bands of phosphate to brushite set up at 1215, 1136, 1070, 985, 877, 660, 586 and 528 cm$^{-1}$ [7].The bands at 1208–988 and 788–526 cm$^{-1}$ attributed to ν3 and ν4 oscillation of phosphate. Weakly peaks at 987 and 877 cm$^{-1}$ allocate to the P-OH extend of $HPO_4^-$.

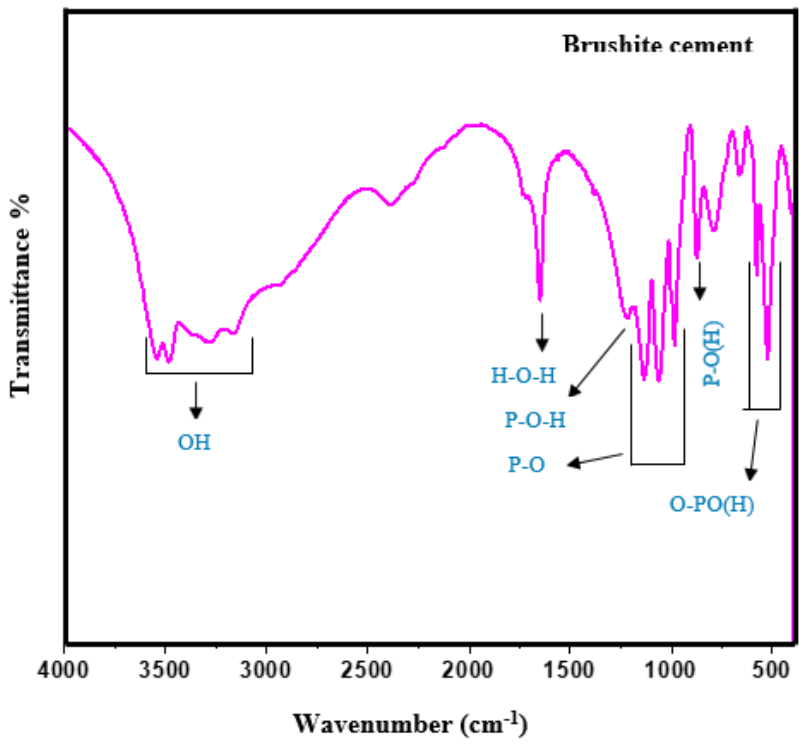


**Figure 3.23:** FT-IR spectra of brushite cement (DPCD)

### 3.11.3 Morphology

Due to the fact that brushite's chemical reactivity is highly dependent on its surface properties, regulating its crystal morphology is crucial for its use as a precursor to other bioceramics or as a functional material. The formation mechanism of nested structures is predicated not only on a reduction in concentration during crystallization, but also on the early aggregation of crystal nuclei. Controlling the early crystallization process, specifically the rate of

nucleation, is thus the most significant determinant in determining the morphology of the brushite crystals. Pure brushite FESEM images revealed the formation of small, irregularly shaped, structured particles (Figure 3.24).

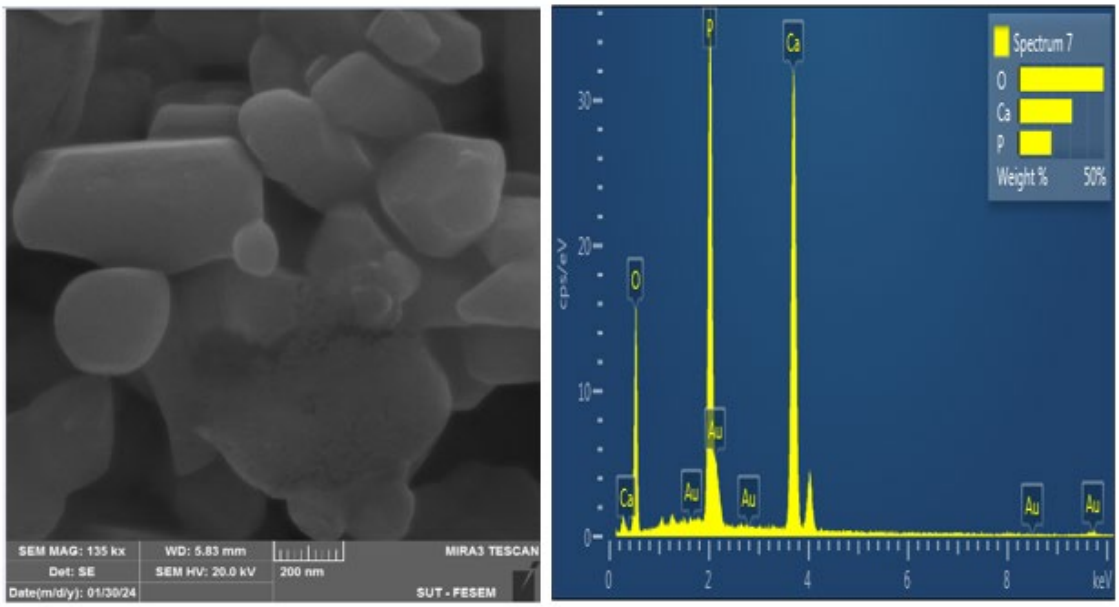


**Figure 3.24.** FESEM images and EDX of brushite cement

## *3.12 In vitro study*

## 3. 12.1 Setting time and injectability

The clinical utility of brushite cements stems from their favorable solubility under physiological conditions. An objective of this study was to ascertain whether the setting reaction has any effect on the injectability of DCPD. Figure 8 illustrates the initial and ultimate configuration periods for DCPD at ambient temperature (25 ◦C). At present, their expansive clinical application is constrained by several

factors: prolonged setting periods, inadequate mechanical strength, and insufficient fluidity to facilitate administration via hypodermic needles. The results of the curing periods, as determined by the Gilmore needle, are depicted in Figure 3.25. The DCPD cement (sample 1) liquid/powder ratio exhibited initial and final curing durations of 2 minutes and 5 minutes, respectively. Brushite cement's rapid curing periods render it inappropriate for use in clinical settings. Conversely, incorporating varying concentrations of trisodium citrate into the brushite cement led to a significant delay in the setting process, as evidenced by the sample 2 final setting time of 7 minutes. Overall, it was observed that the ultimate configuration durations for samples 3, 4, and 5 were 20, 24, and 18 minutes, respectively. The findings suggest that the setting reaction can be influenced by the concentration of trisodium citrate in DCPD, leading to the consistence of DCPD with distinct composite.

Prolonged incorporation at injectable brushite cements into bone remodeling and their enhanced biodegradability make them highly promising as bone replacement materials. While brushite cement can be utilized in minimally invasive procedures, its mechanical strength and injectability are both inadequate. Controlling the injectability of cements and preventing "filter-pressing" of particulate particles and liquid within the syringe. It is recommended that the injection of material occur promptly following the blending of the liquid and granular components of the cement. As shown in Figure 3.25, the injectability of the material rose from 12.22% to 35% (samples 1, 2), and then to 66%, 84%, and 78% (samples 3,4,5), respectively.

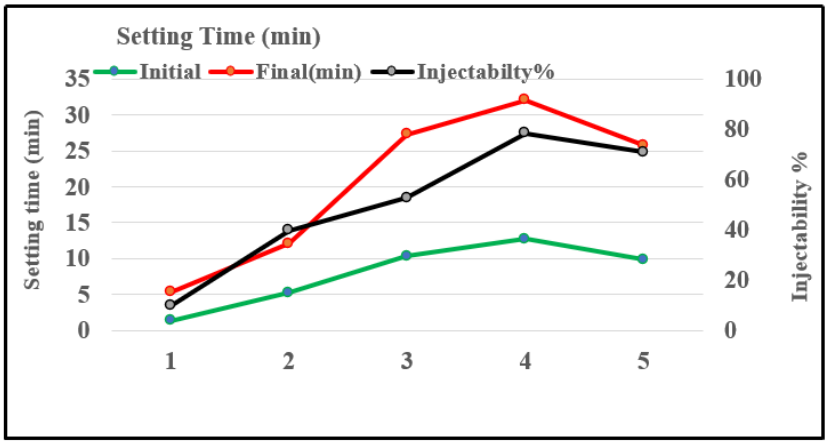


**Figure 3.25.** Setting time and injectability of brushite cements.

## 3.12.2 Compressive strength

Table 3.14 and Figure 3.26 present the compressive strength of brushite cement prior to and subsequent to immersion in SBF for durations of 0, 1, 3, and 7 days. Sample 1 exhibited a compressive strength of 15.58 MPa of brushite prior to immersion in SBF solution. Sample 5's brushite exhibits an increase in compressive strength from 16.93 to 23.87 MPa after 7 days of immersion in SBF. Overall, the Brc's compressive strength increased to 25.34 MPa after three days of marinating in SBF.

**Table 3.14**: Compressive strength (MPa) of brushite

| Samples | 0d | 1d | 3d | 7d | AVERAGE | STDEV |
|---|---|---|---|---|---|---|
| 1 | 0.89 | 5.8 | 10.76 | 15.58 | 8.2575 | 5.48 |
| 2 | 7.88 | 9.87 | 16.92 | 13.47 | 12.035 | 3.45 |
| 3 | 10.78 | 13.63 | 18.83 | 18.28 | 15.38 | 3.33 |
| 4 | 13.45 | 18.34 | 22.45 | 16.76 | 17.75 | 3.23 |
| 5 | 16.93 | 20.78 | 25.34 | 23.87 | 21.73 | 3.22 |

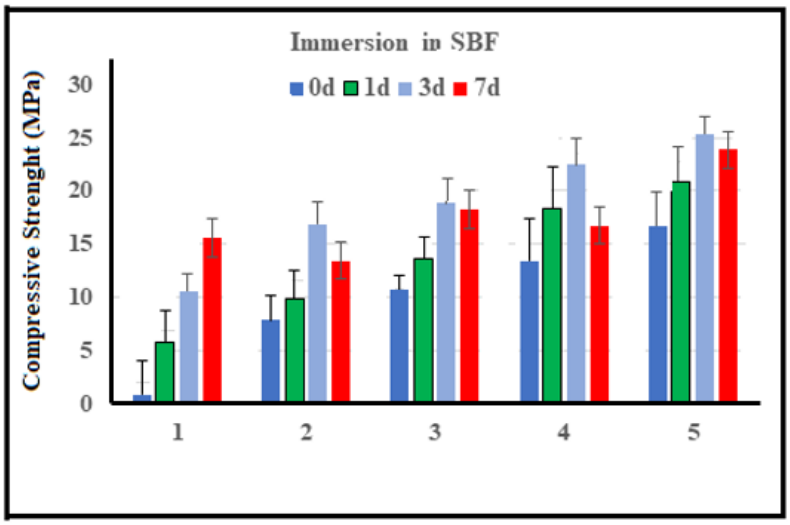


**Figure 3.26**: Compressive strength of brushite before and after immersion in SBF

## 3.13 *In vitro* controlled drug release

### 3.13.1 Antibiotics release profiles from DCPD (DP 900 °C)

Depicted in (Figure 3.27), the cumulative release of cephalexin from DCPD is illustrated. The bimodal release profile was observed in this study, with a surge release occurring within the initial 12 hours, succeeded by a controlled continuous release thereafter. Seven days after the initial rapid release of 55% cephalexin within the first 12 hours, the rate of release slowed and a 73% cumulative release was observed. The gradual speed release of antibiotic was attributed to occurring from within the cement network, as opposed to the initial explosive release which was ascribed to drug release occurring from adsorbed above surface of the samples. To prevent bacterial infection following surgery, a burst release during the initial phase, followed by a gradual release over a period of 7 days, is regarded as an advantageous strategy. The slow release of the antibiotic from cement may be attributed to three potential factors: (i) the formation of an antibiotic-calcium phosphate complex through the interaction of organic acid molecules and calcium ions; (ii) the antibiotic's low water solubility; and (iii) a transformation in the characteristics of the loaded matrix, specifically the transformation of the cement reactants into the apatite phase. Antibiotic molecules could potentially become ensnared in the apatite crystals.

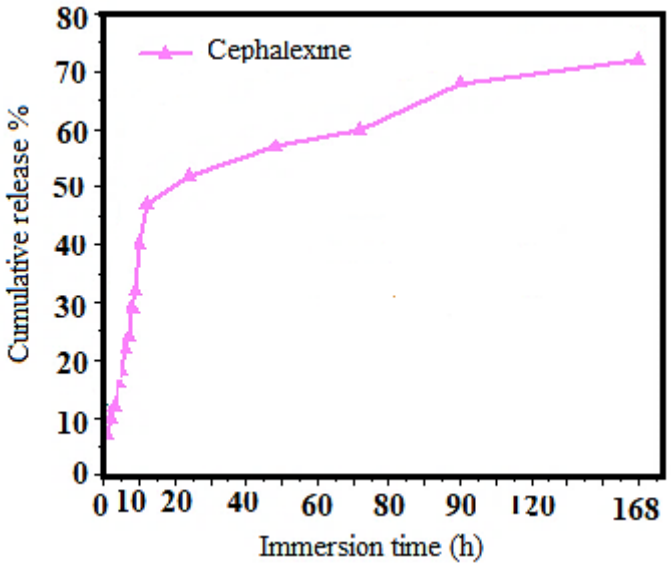


**Figure 3.27:** Antibiotics release profiles from DCPD (DP 900 °C)

# CHAPTER FOUR

# CONCLUSIONS AND RECOMMENDATIONS

## 4 -1 Conclusions

1- The purified phase of the synthesized HA was obtained by calcining bovine and fish bone and analyzing the extracted HA with an FT-IR spectrophotometer, XRD, FESEM, and EDX (affixed to FESEM). The calcination method was effectively utilized to obtain phase pure hydroxyapatite at Ca/P ratio of 1.68.

2- DCPD cements preparing by two phases, HA and MCPM as solid phase and different concentration of trisodium citrate as liquid phase with different ratio, and analyzing the preparing cement with an FT-IR spectrophotometer, XRD, FESEM, and EDX (affixed to FESEM). Study the mechanical properties as setting time, injectability and compressive strength were reported.

3- The avoidance of postoperative bacterial infections is critical to the success of surgical procedures involving the insertion of osteoconductive materials or prostheses. Post-operative infections can be prevented by incorporating antimicrobial agents into DCPD cements, such as antibiotics or other antimicrobial agents. An investigation was conducted into the cumulative release of cephalexin from brushite cement systems. The present analysis reveals a bimodal release profile, characterized by explosive release within the initial 12 hours and a subsequent controlled continuous release thereafter. The gradual sustained release of the drug is ascribed to the drug being released from within the cement network, as opposed to the initial explosive release which is ascribed to the drug being released from adsorbed on the exterior surface of the samples. It is believed that a burst release during the initial phase, followed by a gradual release over the course of seven days, is optimal for preventing bacterial infection following surgery

4- . DCP cements derived from HA exhibited favorable mechanical properties and an in vitro setting reaction in this investigation. Consequently, they exhibit promise as candidates to multitude of biomedical applications. Their ultimate application in biomaterials, however, is contingent on their in vivo biocompatibility and low cytotoxicity.

## 4.2 Recommendations

1. The calcination method was used to extract the HA from three different kind of bones (BB, DP and LN). The three bones used in the present study are good potential candidates for various orthopaedic and dental applications. However, using them as biomaterial depends on good in-vivo biocompatibility and low cytotoxicity.

2. In the present study, HA/MCPM have been used to prepare DCPD cements, which shows good *in vitro* setting reaction, mechanical properties and antibiotic activity and thus they are considered as potential candidates for various orthopaedic and dental applications. However, more investigation is needed to establish osteoblast cells proliferation and their ability to mineralize the bone matrix and thus establishing suitability of these materials as useable biomaterials for such applications.

3. Since it is well known that different bacteria can cause infections in different situations. Thus, it would be crucial to suggest a material that could be combined with several medications so that the surgeon could select the medication right before implantation. Furthermore, a significant obstacle to the application of this technology is that the characteristics of DCPD may be impacted by many medications. To be able to adapt these materials to various therapeutic demands and create repeatable and predictable drug delivery systems, a great deal of work has to go into establishing the general principles that govern the release profile of these kinds of materials.

# REFERENCES

**References**


1. Hertel, R., Fractures of the proximal humerus in osteoporotic bone. *Osteoporosis International*, 2005. 16: p. S65-S72.
2. Razfar, N., Comparison of proximal humeral bone stresses between stemless, short stem, and standard stem length: a finite element analysis. *Journal of shoulder and elbow surgery*, 2016. 25(7): p. 1076-1083.
3. Piccirillo, C., Extraction and characterization of apatite- and tricalcium phosphate-based materials from cod fish bones. *Materials Science and Engineering: C*, 2013. 33(1): p. 103-110.
4. Kumar, A., FEA of humerus bone fracture and healing, *in Advanced Materials for Biomechanical Applications.* 2022, CRC Press. p. 255-272.
5. Nandi, S.K., Orthopedic applications of bone graft & graft substitutes: a review. *Indian Journal of Medical Reseach*, 2010. 132(1): p. 15-30.
6. Schumaier, A. and B. Grawe, Proximal humerus fractures: evaluation and management in the elderly patient. *Geriatric Orthopaedic Surgery & Rehabilitation,* 2018. 9: p. 2151458517750516.
7. Pu'ad, N.A.S.M., Syntheses of hydroxyapatite from natural sources. *Heliyon,* 2019. 5(5): p. e01588.
8. Lertcumfu, N., Properties of calcium phosphates ceramic composites derived from natural materials. *Ceramics International*, 2016. 42(9): p. 10638-10644.

9. O'Hare, P., biological responses to hydroxyapatite surfaces deposited via a co-incident microblasting technique. *Biomaterials*, 2010. 31(3): p. 515-522.

10. Boskey, A.L., *Third Edit. 2013, Elsevier.*

11. Mour, M., Advances in porous biomaterials for dental and orthopaedic applications. *Materials,* 2010. 3(5): p. 2947-2974.

12. Feng, C., Co-inspired hydroxyapatite-based scaffolds for vascularized bone regeneration. *Acta Biomaterialia,* 2021. 119: p. 419-431.

13. Zhang, D., The development of collagen based composite scaffolds for bone regeneration. *Bioactive materials*, 2018. 3(1): p. 129-138.

14. Falconer, J.L. and D.W. Grainger, 1.4 Silver antimicrobial biomaterials. *Compr. Biomater*. II, 2017. 1: p. 79-91.

15. Adzila, S., M. Murad, and I. Sopyan, Doping metal into calcium phosphate phase for better performance of bone implant materials. Recent Patents on *Materials Science*, 2012. 5(1): p. 18-47.

16. Dhandayuthapani, B. and D. Sakthi kumar, Biomaterials for biomedical applications. *Biomedical Applications of Polymeric Materials and Composites,* 2016: p. 1-20.

17. Engstrand, J., C. Persson, and H. Engqvist, The effect of composition on mechanical properties of brushite cements. *Journal of the mechanical behavior of biomedical materials,* 2014. 29: p. 81-90.

18. Dorozhkin, S.V., Calcium orthophosphate cements for biomedical application. *Journal of Materials Science*, 2008. 43(9): p. 3028-3057.

19. Rollo, J.M.D.d.A., Assessment of trabecular bones microarchitectures and crystal structure of hydroxyapatite in bone osteoporosis with application of the Rietveld method. *Procedia Engineering*, 2015. 110: p. 8-14.

20. Bhat, S.V., Biomaterials. 2005: *Alpha Science Int'l Ltd.*

21. Sofronia, A.M., Thermal and structural characterization of synthetic and natural nanocrystalline hydroxyapatite. *Materials Science and Engineering: C,* 2014. 43: p. 153-163.

22. Hoffman, R.M., Patient-derived orthotopic xenografts: better mimic of metastasis than subcutaneous xenografts. *Nature Reviews Cancer*, 2015. 15(8): p. 451-452.

23. Habraken, W., Calcium phosphates in biomedical applications: materials for the future. *Materials Today*, 2016. 19(2): p. 69-87.

24. Mohd Pu'ad, N.A.S., Syntheses of hydroxyapatite from natural sources. *Heliyon*, 2019. 5(5): p. e01588.

25. De Groot, K., Bioceramics Calcium Phosphate. Vol. 226. 2018: *CRC press*.

26. Al-Haddad, A. and Z.A. Che Ab Aziz, Bioceramic-based root canal sealers: a review. *International journal of biomaterials*, 2016. 2016.

27. Moradi, A., M. Pakizeh, and T. Ghassemi, A review on bovine hydroxyapatite; extraction and characterization. *Biomedical Physics & Engineering Express,* 2022. 8(1): p. 012001.

28. Yelten-Yilmaz, A. and S. Yilmaz, Wet chemical precipitation synthesis of hydroxyapatite (HA) powders. *Ceramics International*, 2018. 44(8): p. 9703-9710.

29. Terzioğlu, P., H. Öğüt, and A. Kalemtaş, Natural calcium phosphates from fish bones and their potential biomedical applications. *Materials Science and Engineering: C*, 2018. 91: p. 899-911.

30. Zakaria, S.M., Nanophase hydroxyapatite as a biomaterial in advanced hard tissue engineering: a review. *Tissue Engineering Part B: Reviews,* 2013. 19(5): p. 431-441.

31. Piccirillo, C., Hydroxyapatite-based materials of marine origin: A bioactivity and sintering study. *Materials Science and Engineering: C*, 2015. 51: p. 309-315.

32. Ni, Z., et al., Synthesis of silver nanoparticle-decorated hydroxyapatite (HA@ Ag) poriferous nanocomposites and the study of their antibacterial activities. *RSC advances,* 2018. 8(73): p. 41722-41730.

33. Bahrololoom, M.E., Characterization of natural hydroxyapatite extracted from bovine cortical bone ash. *J. Ceram. Process. Res*, 2009. 10(2): p. 129-138.

34. Sallemi, I., F.B. Ayed, and J. Bouaziz. Effect of fluorapatite additive on the mechanical properties of tricalcium phosphate-zirconia composites. *IOP Publishing.*

35. Yokoi, T., Hydroxyapatite formation from octacalcium phosphate and its related compounds: a discussion of the transformation mechanism. *Bulletin of the Chemical Society of Japan*, 2020. 93(5): p. 701-707.

36. Lawton, D.M., M.D.J. Lamaletie, and D.L. Gardner, Biocompatibility of hydroxyapatite ceramic: response of chondrocytes in a test system using low temperature scanning electron microscopy. *Journal of Dentistry*, 1989. 17(1): p. 21-27.

37. Pramanik, N., Chemical synthesis, characterization, and biocompatibility study of hydroxyapatite/chitosan phosphate nanocomposite for bone tissue engineering applications. *International journal of biomaterials*, 2009.

38. Do Prado Ribeiro, D.C., Study of the osteoconductive capacity of hydroxyapatite implanted into the femur of ovariectomized rats. *Microscopy research and technique*, 2012. 75(2): p. 133-137.

39. Jaramillo, C.D., Osteoconductive and osseointegration properties of a commercial hydroxyapatite compared to a synthetic product. *Revista Colombiana de Ciancia's Peccaries*, 2010. 23(4): p. 471-483.

40. Jang, H.L., Phase transformation from hydroxyapatite to the secondary bone mineral, whitlockite. *Journal of materials chemistry* B, 2015. 3(7): p. 1342-1349.

41. Brown, W.E. and L.C. Chow, Chemical properties of bone mineral. Annual *Review of Materials Science*, 1976. 6(1): p. 213-236.

42. Ayatollah, M.R., Mechanical and tribological properties of hydroxyapatite nanoparticles extracted from natural bovine bone and the bone cement

developed by nano-sized bovine hydroxyapatite filler. *Ceramics International*, 2015. 41(9, Part A): p. 10818-10827.

43. Venkatesan, J., Isolation and characterization of nano-hydroxyapatite from salmon fish bone. *Materials,* 2015. 8(8): p. 5426-5439.

44. Sun, R.-X., Physicochemical and biological properties of bovine-derived porous hydroxyapatite/collagen composite and its hydroxyapatite powders. *Ceramics International,* 2017. 43(18): p. 16792-16798.

45. Londoño-Restrepo, S.M., Study of bovine hydroxyapatite obtained by calcination at low heating rates and cooled in furnace air. *Journal of Materials Science,* 2016. 51(9): p. 4431-4441.

46. Oladele, I.O., non-synthetic sources for the development of hydroxyapatite. *J. Appl. Biotechnol. Bioeng*, 2018. 5(2): p. 88-95.

47. Kabilan, N., Optical nonlinear properties of hydroxyapatite-based *materials. Optik*, 2022. 265: p. 169562.

48. Jaber, H.L., A.S. Hammood, and N. Parvin, Synthesis and characterization of hydroxyapatite powder from natural Camelus bone. *Journal of the Australian Ceramic Society*, 2018. 54(1): p. 1-10.

49. Doostmohammadi, A., A comparative physico-chemical study of bioactive glass and bone-derived hydroxyapatite. *Ceramics International*, 2011. 37(5): p. 1601-1607.

50. Fudge, E.A., Synthesis of organic derived hydroxyapatite scaffold from pig bone waste for tissue engineering applications. *Advanced Powder Technology,* 2018. 29(1): p. 1-8.

51. López, E.O., Hydroxyapatite and lead-substituted hydroxyapatite near-surface structures: Novel modelling of photoemission lines from X-ray photoelectron spectra. *Applied Surface Science*, 2022. 571: p. 151310.

52. Panda, N.N., K. Pramanik, and L.B. Sukla, Extraction and characterization of biocompatible hydroxyapatite from fresh water fish scales for tissue engineering scaffold. *Bioprocess and Biosystems Engineering,* 2014. 37(3): p. 433-440.

53. DileepKumar, V.G., A review on the synthesis and properties of hydroxyapatite for biomedical applications. *Journal of Biomaterials Science, Polymer Edition,* 2022. 33(2): p. 229-261.

54. Sunil, B.R. and M. Jagannatham, Producing hydroxyapatite from fish bones by heat treatment. *Materials Letters,* 2016. 185: p. 411-414.

55. Hidouri, M., S.V. Dorozhkin, and N. Albeladi, Thermal behavior, sintering and mechanical characterization of multiple ion-substituted hydroxyapatite bioceramics. *Journal of Inorganic and Organometallic Polymers and Materials*, 2019. 29: p. 87-100.

56. Neelakandeswari, N., G. Sangami, and N. Dharmaraj, Preparation and characterization of nanostructured hydroxyapatite using a biomaterial. Synthesis and Reactivity in Inorganic, *Metal-Organic, and Nano-Metal Chemistry*, 2011. 41(5): p. 513-516.

57. Bano, N., Natural hydroxyapatite extracted from bovine bone. *Journal of Science and Technology,* 2017. 9(2).

58. Hussin, M.S.F., Extraction of natural hydroxyapatite for biomedical applications—A review. Heliyon, 2022: p. e10356.

59. Akram, M., Extracting hydroxyapatite and its precursors from natural resources. *Journal of Materials Science*, 2014. 49(4): p. 1461-1475.

60. Sihn, Y., Cation-exchanged hydroxyapatite for strontium separation from groundwater. 2021.

61. Herliansyah, M.K., Preparation and characterization of natural hydroxyapatite: a comparative study of bovine bone hydroxyapatite and hydroxyapatite from calcite. *Trans Tech Publ.*

62. Ayatollahi, M.R., Mechanical and tribological properties of hydroxyapatite nanoparticles extracted from natural bovine bone and the bone cement developed by nano-sized bovine hydroxyapatite filler. *Ceramics International*, 2015. 41(9): p. 10818-10827.

63. Ruksudjarit, A., Synthesis and characterization of nanocrystalline hydroxyapatite from natural bovine bone. *Current applied physics*, 2008. 8(3-4): p. 270-272.

64. Khurshid, Z., Extraction of Hydroxyapatite from Camel Bone for Bone Tissue Engineering Application. *Molecules,* 2022. 27(22): p. 7946.

65. Le Ho, K.H., Physicochemical properties, acute and subchronic toxicity of nano-hydroxyapatite obtained from Lates calcarifer fish bone. *Regional Studies in Marine Science*, 2022. 55: p. 102560.

66. Indra, A., Behavior of sintered body properties of hydroxyapatite ceramics: effect of uniaxial pressure on green body fabrication. *Materials Today Sustainability*, 2022. 17: p. 100100.

67. Indra, A., A novel fabrication procedure for producing high strength hydroxyapatite ceramic scaffolds with high porosity. *Ceramics International*, 2021. 47(19): p. 26991-27001.

68. Odusote, J.K., Synthesis and characterization of hydroxyapatite from bovine bone for production of dental implants. *Journal of applied biomaterials & functional materials*, 2019. 17(2): p. 2280800019836829.

69. Taufik S, A., Treatment of bone defects with bovine hydroxyapatite xenograft and platelet rich fibrin (PRF) to accelerate bone healing. *International Journal of Surgery Case Reports*, 2022. 97: p. 107370.

70. Azzallou, R., Bovine bone-derived natural hydroxyapatite-supported $ZnCl_2$ as a sustainable high efficiency heterogeneous biocatalyst for synthesizing amidoalkyl naphthols. *Journal of Physics and Chemistry of Solids,* 2022. 163: p. 110533.

71. Han, K.-S., Wound healing efficacy of biocompatible hydroxyapatite from bovine bone waste for bone tissue engineering application. *Journal of Environmental Chemical Engineering*, 2022. 10(1): p. 106888.

72. Pazourková, L., G.S. Martynková, and M. Šupová, Ca-deficient hydroxyapatite synthesis on the bioapatite bovine bone substrate study. *Materials Today: Proceedings*, 2022. 52: p. 227-231.

73. Londoño-Restrepo, S.M., The effect of cyclic heat treatment on the physicochemical properties of bio hydroxyapatite from bovine bone. *Journal of Materials Science: Materials in Medicine*, 2018. 29: p. 1-15.

74. Pires, L.A., Effects of ZnO/TiO2 nanoparticle and TiO2 nanotube additions to dense polycrystalline hydroxyapatite bioceramic from bovine bones. *Dental Materials*, 2020. 36(2): p. e38-e46.

75. Surya, P., Synthesis and characterization of nano-hydroxyapatite from Sardinella longiceps fish bone and its effects on human osteoblast bone cells. *Journal of the Mechanical Behavior of Biomedical Materials*, 2021. 119: p. 104501.

76. Hasan, M.R., N.S.M. Yasin, and M.S. Mohd, Proximate and morphological characteristics of nano hydroxyapatite (Nano HA extracted from fishbone. *Journal of Sustainability Science and Management*, 2020. 15(8): p. 9-21.

77. Venkatesan, J., Isolation and Characterization of Nano-Hydroxyapatite from Salmon Fish Bone. *Materials (Basel),* 2015. 8(8): p. 5426-5439.

78. Pal, A., Synthesis of hydroxyapatite from Lates calcarifer fish bone for biomedical applications. *Materials Letters*, 2017. 203: p. 89-92.

79. Shi, P., Characterization of natural hydroxyapatite originated from fish bone and its biocompatibility with osteoblasts. *Materials Science and Engineering: C,* 2018. 90: p. 706-712.

80. Ahmad Fara, A.N.K., M.A. bin Yahya, and H.Z. Abdullah. Preparation and characterization of biological hydroxyapatite (HA) obtained from Tilapia fish bone. *Trans Tech Publ*.

81. Popescu-Pelin, G., Fish bone derived bi-phasic calcium phosphate coatings fabricated by pulsed laser deposition for biomedical applications. *Marine drugs*, 2020. 18(12): p. 623.

82. Elango, J., Rheological, biocompatibility and osteogenesis assessment of fish collagen scaffold for bone tissue engineering. *International Journal of Biological Macromolecules*, 2016. 91: p. 51-59.

83. Pon-On, W., Hydroxyapatite from fish scale for potential use as bone scaffold or regenerative material. *Materials Science and Engineering: C,* 2016. 62: p. 183-189.

84. Manalu, J., B. Soegijono, and D. Indrani, Characterization of Hydroxyapatite Derived from Bovine Bone. 2015.

85. Sathiyavimal, S., Natural organic and inorganic–hydroxyapatite biopolymer composite for biomedical applications. *Progress in Organic Coatings,* 2020. 147: p. 105858.

86. Ribeiro, N., new prospects in skin regeneration and repair using nanophased hydroxyapatite embedded in collagen nanofibers. *Nanomedicine: Nanotechnology, Biology and Medicine*, 2021. 33: p. 102353.

87. Bano, N., Extraction of biological apatite from cow bone at different calcination temperatures: a comparative study. *Key Engineering Materials*, 2019. 796: p. 46-52.

88. Mondal, S., Studies on Processing and Characterization of Hydroxyapatite Biomaterials from Different Bio Wastes. *Journal of Minerals and Materials Characterization and Engineering,* 2012. 11: p. 55-67.

89. Zhang, L., Extraction and characterization of HA/β-TCP biphasic calcium phosphate from marine fish. *Materials Letters*, 2019. 236: p. 680-682.

90. Balamurugan, A., Suitability evaluation of sol–gel derived Si-substituted hydroxyapatite for dental and maxillofacial applications through in vitro osteoblasts response. *Dental Materials*, 2008. 24(10): p. 1374-1380.

91. Walsh, P.J., Low-pressure synthesis and characterization of hydroxyapatite derived from mineralize red algae. *Chemical Engineering Journal,* 2008. 137(1): p. 173-179.

92. Monballiu, A., Phosphate recovery as hydroxyapatite from nitrified UASB effluent at neutral pH in a CSTR. *Journal of Environmental Chemical Engineering,* 2018. 6(4): p. 4413-4422.

93. Govindaraj, D. and M. Rajan, Synthesis and Spectral Characterization of Novel Nano-Hydroxyapatite from Moringaoleifera Leaves. *Materials Today: Proceedings*, 2016. 3(6): p. 2394-2398.

94. Salma-Ancane, K., L. Stipniece, and Z. Irbe, Effect of biogenic and synthetic starting materials on the structure of hydroxyapatite bioceramics. *Ceramics International*, 2016. 42(8): p. 9504-9510.

95. Tarafdar, A., Advances in biomaterial production from animal derived waste. *Bioengineered*, 2021. 12(1): p. 8247-8258.

96. Deng, K., Preparation and characterization of porous HA/β-TCP biphasic calcium phosphate derived from butterfish bone. *Materials Technology,* 2022. 37(10): p. 1388-1395.

97. Huang, Y.-C., P.-C. Hsiao, and H.-J. Chai, Hydroxyapatite extracted from fish scale: Effects on MG63 osteoblast-like cells. *Ceramics International*, 2011. 37(6): p. 1825-1831.

98. Shaltout, A.A., M.A. Allam, and M.A. Moharram, FTIR spectroscopic, thermal and XRD characterization of hydroxyapatite from new natural sources. Spectrochemical Acta Part A: *Molecular and Biomolecular Spectroscopy*, 2011. 83(1): p. 56-60.

99. Rabiei, M., Comparing methods for calculating nano crystal size of natural hydroxyapatite using X-ray diffraction. *Nanomaterials,* 2020. 10(9): p. 1627.

100. Plumbum, I., Synthesis and characterization of hydroxyapatite from bulk seashells and its potential usage as lead ions adsorbent. *Malaysian Journal of Analytical Sciences*, 2017. 21(3): p. 571-584.

101. Vallet-Regí, M. and J.M. González-Calbet, Calcium phosphates as substitution of bone tissues. *Progress in Solid State Chemistry*, 2004. 32(1): p. 1-31.

102. Klinkaewnarong, J. and S. Utara, Ultrasonic-assisted conversion of limestone into needle-like hydroxyapatite nanoparticles. *Ultrasonics Sonochemistry,* 2018. 46: p. 18-25.

103. Wu, S.-C., A hydrothermal synthesis of eggshell and fruit waste extract to produce nanosized hydroxyapatite. *Ceramics International,* 2013. 39(7): p. 8183-8188.

104. Ofudje, E.A., Nano-rod hydroxyapatite for the uptake of nickel ions: Effect of sintering behavior on adsorption parameters. *Journal of Environmental Chemical Engineering,* 2021. 9(5): p. 105931.

105. Sharma, C., Fabrication and characterization of novel nano-biocomposite scaffold of chitosan–gelatin–alginate–hydroxyapatite for bone tissue engineering. *Materials Science and Engineering: C*, 2016. 64: p. 416-427.

106. Bayar, N., M. Kriaa, and R. Kammoun, Extraction and characterization of three polysaccharides extracted from Opuntia ficus indica cladodes. *International Journal of Biological Macromolecules*, 2016. 92: p. 441-450.

107. Aarthy, S., Exploring the effect of sintering temperature on naturally derived hydroxyapatite for bio-medical applications. *Journal of Materials Science: Materials in Medicine*, 2019. 30: p. 1-11.

108. Jindapon, N., Preparation, Characterization, and Biological Properties of Hydroxyapatite from Bigeye Snapper (Priancanthus tayenus) Bone. *International Journal of Molecular Sciences*, 2023. 24(3): p. 2776.

109. Grassino, A.N., Ultrasound assisted extraction and characterization of pectin from tomato waste. *Food chemistry,* 2016. 198: p. 93-100.

110. Alici, E.H., Alkyl chain modified metal phthalocyanines with enhanced antioxidant-antimicrobial properties by doping $Ag^{+}$ and $Pd^{2+}$ ions. *Journal of Molecular Structure*, 2022. 1257: p. 132634.

## الخلاصة

تنقسم الرسالة إلى ثلاثة فصول. يقدم الفصل الأول لمحة واسعة عن استخراج الهيدروكسيباتيت البيولوجي من المصادر الطبيعية لاستخدامه في التطبيقات الطبية الحيوية. في الفصل الثاني يتم تحضير العينة، واستخلاص الهيدروكسيباتيت، وتصنيع أسمنت فوسفات الكالسيوم . تتم تغطية النتائج والتعليقات في الفصل الأخير. استخدم هذا البحث مجموعة متنوعة من الهيدروكسيباتيت المستخرج حديثاً من عظام الأسماك في الخليج العربي بالبصرة، العراق، وعظام الأبقار من مدينة ميسان، العراق، كمصادر طبيعية للعظام. وذلك باستخدام عملية التكليس عند درجات حرارة مختلفة. نظرًا لقدرتها على إعادة الامتصاص في ظل الظروف الفسيولوجية، غالبًا ما يتم اختيار أسمنت فوسفات الكالسيوم (CPC) بدلاً من المواد الحيوية البديلة المعتمدة على فوسفات الكالسيوم في إجراءات جراحة العظام. تركز تقنيات تطوير الأسمنت الحالية لفوسفات الكالسيوم على وضع الأسمنت في الموقع تحت ظروف فسيولوجية ذات خصائص ميكانيكية مناسبة. تم تشخيص تكوين الطور، والتشكل السطحي، والتركيب الكيميائي لأسمنت فوسفات الكالسيوم وهيدروكسيباتيت (HA) عن طريق حيود الأشعة السينية(XRD) ، والمجهر الإلكتروني لمسح الانبعاثات الميدانية (FESEM) إلى جانب تحليل الأشعة السينية المشتتة من الطاقة (EDX) تقنيات التحليل الطيفي للأشعة تحت الحمراء، والأشعة السينية، .(FTIR) قمنا بتقييم سلوك تشبع الأسمنت في المختبر عن طريق غمر العينات في سوائل الجسم المحاكية (SBF) لمدة سبعة أيام عند 37 درجة مئوية.

جمهورية العراق

وزارة التعليم العالي والبحث العلمي

جامعة ميسان

كلية العلوم

قسم الكيمياء

# تحضير أسمنت فوسفات الكالسيوم المستخرج من الأسماك البحرية وعظام الابقار القابل للحقن لتطبيقات الجراحة العظمية

رسالة مقدمة الى

**كلية العلوم / جامعة ميسان جزء من متطلبات نيل شهادة الماجستير في علوم الكيمياء**

من قبل الطالبة

**خلود جبار والي**

بكالوريوس علوم كيمياء / جامعة البصره ( 2002 )

بإشراف

**الأستاذ المساعد الدكتور علي طه صالح**

2024